# FGF7 is a functional niche signal required for stimulation of adult liver progenitor cells that support liver regeneration

**Hinako M. Takase,[1,5,6] Tohru Itoh,[1,5,7] Seitaro Ino,[1] Ting Wang,[2] Takehiko Koji,[3] Shizuo Akira,[4] Yasuhiro Takikawa,[2] and Atsushi Miyajima[1]**

[1]Laboratory of Cell Growth and Differentiation, Institute of Molecular and Cellular Biosciences, The University of Tokyo, Tokyo 113-0032, Japan; [2]Division of Gastroenterology and Hepatology, Department of Internal Medicine, Iwate Medical University, Iwate 020-8505, Japan; [3]Department of Histology and Cell Biology, Nagasaki University Graduate School of Biomedical Sciences, Nagasaki 852-8523, Japan; [4]Laboratory of Host Defense, World Premier International Immunology Frontier Research Center, Osaka University, Osaka 565-0871, Japan

**The liver is a unique organ with a remarkably high potential to regenerate upon injuries. In severely damaged livers where hepatocyte proliferation is impaired, facultative liver progenitor cells (LPCs) proliferate and are assumed to contribute to regeneration. An expansion of LPCs is often observed in patients with various types of liver diseases. However, the underlying mechanism of LPC activation still remains largely unknown. Here we show that a member of the fibroblast growth factor (FGF) family, FGF7, is a critical regulator of LPCs. Its expression was induced concomitantly with LPC response in the liver of mouse models as well as in the serum of patients with acute liver failure. *Fgf7*-deficient mice exhibited markedly depressed LPC expansion and higher mortality upon toxin-induced hepatic injury. Transgenic expression of FGF7 in vivo led to the induction of cells with characteristics of LPCs and ameliorated hepatic dysfunction. We revealed that Thy1$^+$ mesenchymal cells produced FGF7 and appeared in close proximity to LPCs, implicating a role for those cells as the functional LPC niche in the regenerating liver. These findings provide new insights into the cellular and molecular basis for LPC regulation and identify FGF7 as a potential therapeutic target for liver diseases.**

[*Keywords*: liver regeneration; progenitor cells; niche signal; FGF7; Thy1$^+$ cells]

Supplemental material is available for this article.

Received August 31, 2012; revised version accepted December 13, 2012.

In the liver, hepatocytes and cholangiocytes (bile duct epithelial cells [BECs]) are the only two epithelial cell lineages among various types of the constituent cells. Cells that give rise to both hepatocytes and BECs are generally regarded as bipotential liver progenitors or stem cells. In liver development, hepatoblasts emerging from the foregut endoderm fulfill this criterion and are thus considered to be fetal liver stem/progenitor cells (Tanimizu and Miyajima 2007). During adult liver homeostasis, liver maintenance is achieved by cell division of mature hepatocytes and BECs (Ponder 1996). It is important to note that the adult liver can regenerate under conditions of massive parenchymal loss. After surgical removal or partial hepatectomy (PHx), residual mature hepatocytes restore the liver mass. The contribution of liver stem/progenitor cells to regeneration seems to be minimal if any in this type of liver injury (Michalopoulos and DeFrances 1997), although several recent studies have suggested the presence of newborn hepatocytes originating from sources other than pre-existing hepatocytes (Furuyama et al. 2011; Iverson et al. 2011; Malato et al. 2011). In contrast, when the liver is severely damaged, as in the case of hepatocyte-selective proliferation defect caused by some drugs or toxins, the contribution of adult liver progenitor cells (LPCs) is assumed (Fausto 2004; Knight et al. 2005; Bird et al. 2008; Duncan et al. 2009). The LPCs are a cell population with a high nuclear/cytoplasmic ratio and are known as "oval cells" in rodent models because of their ovoid appearance (Farber 1956). Upon liver damage, LPCs emerge from periportal regions, proliferate extensively, migrate into the hepatic lobule, and are considered to differentiate into both hepatocytes and BECs (Fausto 2004; Knight et al. 2005). As these types of progenitor cells are not observed in the uninjured liver, they are

[5]**These two authors contributed equally to this work.**
[6]**Present address: Howard Hughes Medical Institute, Department of Developmental Biology, Stanford University, School of Medicine, Stanford, CA 94035, USA.**
[7]**Corresponding author**
**E-mail itohru@iam.u-tokyo.ac.jp**
Article published online ahead of print. Article and publication date are online at http://www.genesdev.org/cgi/doi/10.1101/gad.204776.112.

often referred to as facultative stem/progenitor cells in the adult liver (Alison et al. 1996; Yanger and Stanger 2011).

There are several experimental models to induce LPCs. In mice, 3,5-diethoxycarbonyl-1,4-dihydrocollidine (DDC) diet and choline-deficient, ethionine-supplemented (CDE) diet models are often used (Preisegger et al. 1999; Akhurst et al. 2001). The LPC response, also termed as ductular reaction, has been found in human chronic liver diseases and severely injured livers, such as acute hepatitis, fulminant hepatitis, cholestatic disorders, and liver cancers (Libbrecht and Roskams 2002; Turanyi et al. 2010). This suggests that LPCs are broadly activated to restore the function of the liver when mature hepatocytes fail to proliferate. Despite previous notions that the degree of the LPC response correlates with the severity of liver disease (Lowes et al. 1999), it has not been demonstrated whether LPCs indeed engage in liver regeneration. In addition, the underlying mechanism of the activation of LPCs still remains largely unknown.

As liver injuries accompanying the LPC responses are usually associated with inflammation and fibrosis, interaction between LPCs and multiple other cell populations, such as immune cells and fibroblastic cells, has been postulated. In many cases of adult stem/progenitor cell regulation, the importance of the extracellular signals provided by the surrounding cells, forming the so-called stem cell niche, are well recognized. However, little has been documented as to whether and how the LPCs are regulated by the niche signals. Cell-to-cell interactions involve paracrine growth factors and cytokines that can be grouped into several major families (Gerhart 1999), among which the fibroblast growth factor (FGF) family is one of the best characterized. FGFs constitute a family of growth factors that have diverse activities in development and adulthood. It has been reported that FGF signals participate in tissue development and organization, branching morphogenesis, angiogenesis, and wound repair, as well as the regulation of stem cell systems in various organs (Itoh and Ornitz 2008; Turner and Grose 2010). The mammalian FGF family is classified as paracrine (canonical) ligands, endocrine ligands, and FGF homologous factors. The paracrine FGF families can be further subdivided into five subfamilies—FGF1/2, FGF3/7/10/22, FGF4/5/6, FGF8/17/18, and FGF9/16/20—in mice and humans. There are four members of the FGF receptor family: FGFR1, FGFR2, FGFR3, and FGFR4. Since FGFR1, FGFR2, and FGFR3 each have splice variant isoforms "b" and "c," seven different FGFR subtypes can be expressed. It is known that their specific functions are achieved by spatially and temporally regulated expression patterns of particular ligands and receptors; for example, the FGF3/7/10/22 subfamily ligands are typically expressed by mesenchymal cells and exert their effects through the cognate receptor FGF receptor 2 isoform IIIb (FGFR2b), whose expression is restricted in epithelial cells (Steiling and Werner 2003).

In the present study, we aimed at elucidating the cellular and molecular framework that underlies the LPC regulation upon liver injury. Based on the characteristic expression profile and the results of in vivo functional analyses, we found evidence that FGF7 is an essential signal for induction of the LPC response and contributes to the progenitor-dependent liver regeneration.

## Results

### *Thy1$^+$ cell population is a candidate for the LPC niche*

As previous studies have suggested that nonepithelial populations such as mesenchymal cells and immune cells reside near and around LPCs (Paku et al. 2001; Knight et al. 2007; Strick-Marchand et al. 2008), we suspected that those cells may functionally interact with LPCs and provide a putative LPC niche. To identify and characterize such an LPC–niche interaction, we first induced the LPC response in the mouse liver with a well-established protocol of the hepatotoxin DDC diet application (Preisegger et al. 1999). Cytokeratin 19$^+$ (CK19$^+$) LPCs expanded from around the portal vein after liver damage by feeding DDC diet (Fig. 1A). Immunostaining of the liver sections with several cell surface markers led to the finding that a Thy1$^+$ cell population appeared in close proximity to LPCs in DDC-induced liver damage (Fig. 1A). We selected and focused on this marker for further analysis, as its expression in injured livers has also been described in rats and humans (Dezso et al. 2007; Yovchev et al. 2009). An established marker for fibroblastic cells (Elastin) and a stellate cell marker (Desmin) partially overlapped with the Thy1$^+$ area (Supplemental Fig. S1A,B). Quantitative analysis of the Thy1 and CK19 immunostaining revealed that the expansion of Thy1$^+$ cells occurred prior to LPC activation (Fig. 1B). Thus, we presumed that Thy1$^+$ cells could provide a niche for LPCs that allows them to proliferate.

We sought to identify the nature of the niche signals for LPCs possibly provided by Thy1$^+$ cells. Among several major groups of paracrine factors, we especially focused on the FGF family because an LPC-specific marker, Trop2 (Okabe et al. 2009), has previously been reported as a target gene of FGF10 in lung development (Lu et al. 2005). We analyzed expression patterns of all of the paracrine *Fgf* ligands and found *Fgf7* to be highly expressed, while we could not detect any expression of *Fgf10* or *Fgf3/22* belonging to the same subfamily (Supplemental Fig. S2). The expression of *Fgf7* was increased significantly during the time course of DDC-induced liver damage, along with that of *Epcam* and *Krt19*, encoding the LPC/BEC markers epithelial cell adhesion molecule (EpCAM) and CK19, respectively (Fig. 1C). Accordingly, expression of FGF7 protein was barely detected in normal livers but was markedly induced in the vicinity of LPCs after DDC (Fig. 1D,F). Intriguingly, some Thy1$^+$ cells costained with FGF7 in the injured liver (Fig. 1E). We also examined a recovery model for liver injury, where mice were initially fed a DDC diet for 4 wk and then returned to the normal diet for another 2 wk (Supplemental Fig. S3). In this injury/recovery setting, the overall level of *Fgf7* expression strongly correlated with that of the LPC response as well as the progression of liver damage as measured by serum markers. These results suggest that FGF7 is a strong candidate for the niche signal for LPCs.

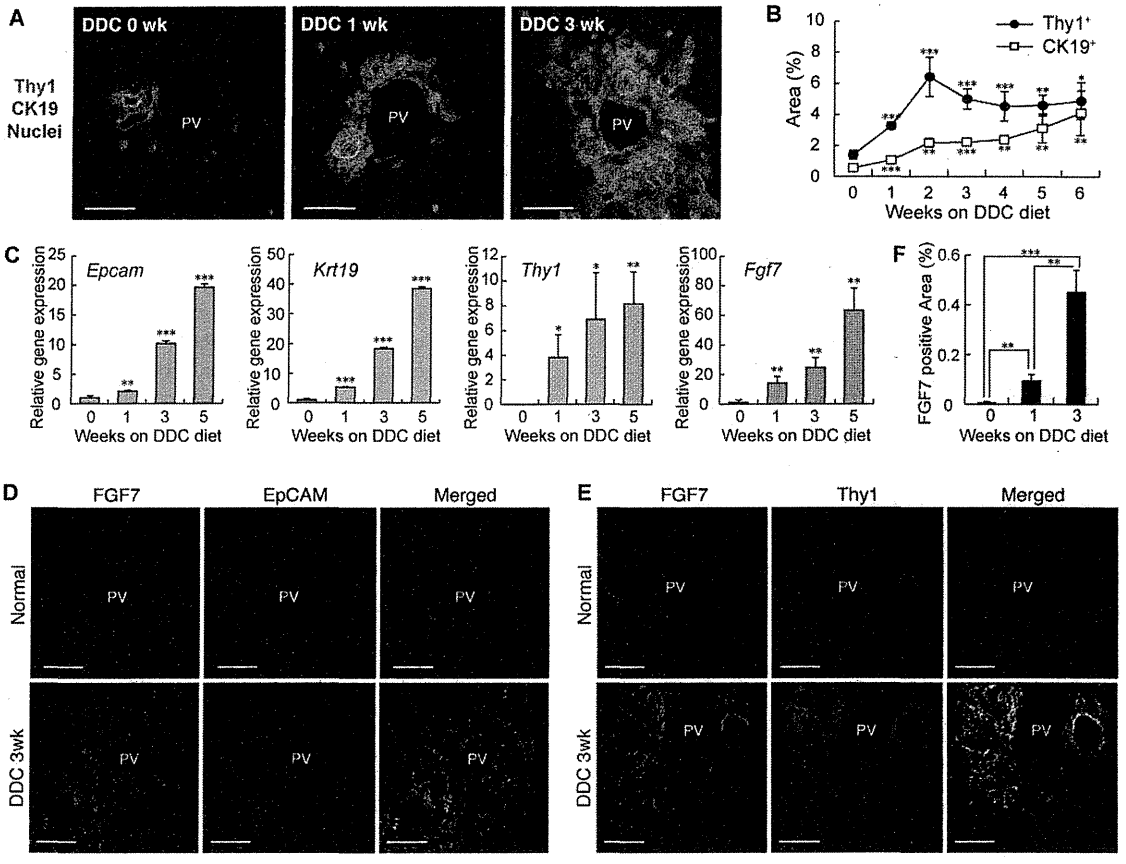


**Figure 1.** FGF7 expression in the damaged liver is up-regulated around LPCs. (*A*) Liver sections prepared from DDC diet-fed mice were subjected to immunofluorescent double-staining analysis. Thy1$^+$ cells (green) were observed in the immediate vicinity of CK19$^+$ LPCs (red) during the course of LPC activation. Bars, 80 μm. (PV) Portal vein. (*B*) Thy1- and CK19-positive areas were increased in the DDC-treated livers, as determined by quantitative analysis of immunofluorescence-stained images. Mean ± SD ($n = 3$). (***) $P < 0.001$; (**) $P < 0.01$; (*) $P < 0.05$, compared with normal liver (0 wk). (*C*) Total RNA was isolated from whole-liver samples of normal diet-fed (0 wk) or DDC diet-fed mice, reverse-transcribed, and subjected to quantitative PCR analyses to determine expression of the LPC markers *Epcam* and *Krt19*, the mesenchymal cell marker *Thy1*, and *Fgf7*. Expression was normalized to that of *Gapdh*. Mean ± SD ($n = 3$). (***) $P < 0.001$; (**) $P < 0.01$; (*) $P < 0.05$, compared with the value at 0 wk. (*D,E*) Confocal immunofluorescence images of the livers show that FGF7 (green) protein localized in the proximity of EpCAM$^+$ LPCs (*D*, red) and colocalized with Thy1$^+$ mesenchymal cells (*E*, red) in the periportal region in injured livers. Bars, 50 μm. (PV) Portal vein. (*F*) Expression of FGF7 protein was increased in the DDC-treated livers, as determined by quantitative analysis of immunofluorescence-stained images of at least 11 periportal fields from three livers for each time point. Mean ± SE. (***) $P < 0.001$; (**) $P < 0.01$.

### *LPCs receive the FGF7 signal from Thy1$^+$ mesenchymal cells*

To determine whether FGF7 can act on LPCs directly, we analyzed the expression of the FGF7 receptor FGFR2b in LPCs. In situ hybridization analysis of liver sections detected expression of the *Fgfr2* transcript in the CK19$^+$ LPC population (Fig. 2A). To validate expression of the cognate isoform for FGF7, EpCAM$^+$ LPCs and EpCAM$^-$ cells were isolated from the nonparenchymal cell (NPC) population of the DDC-treated liver and immunostained with a IIIb isoform-specific anti-FGFR2 antibody. We detected strong expression of FGFR2b in EpCAM$^+$ cells but not in EpCAM$^-$ cells (Fig. 2B,C).

We next performed quantitative PCR analysis using specific cell populations to further confirm the FGF7-producing cells and their target cells. Hepatocyte, NPC, EpCAM$^+$ LPC, Thy1$^+$ CD45$^-$ cell (Thy1$^+$ MC [for mesenchymal cell]) (see below), Thy1$^+$ CD45$^+$ cell (T-cell), and Thy1$^-$ CD45$^+$ cell (blood cell) fractions were isolated from the livers of mice fed DDC. We checked for adequate cell separation by the specific expression of each marker (Supplemental Fig. S3A). As expected from the aforementioned immunostaining patterns, *Fgf7* and *Fgfr2* isoform IIIb were detected in Thy1$^+$ MC and LPC fractions, respectively (Fig. 2D). These results suggest that FGF7 signal may function directionally from Thy1$^+$ CD45$^-$ cells to LPCs. The Thy1$^+$ CD45$^-$ cells strongly expressed *Elastin* (*Eln*), *nerve growth factor receptor* (*Ngfr*; p75NTR) and *α smooth muscle actin* (*Acta2*; α-SMA), which are markers for fibroblastic cells, hepatic stellate cells, and myofibroblasts, respectively (Fig. 2D; Supplemental Fig. S4A). Thus, they are considered to be a mesenchymal cell population and distinct from T-cell populations. We also

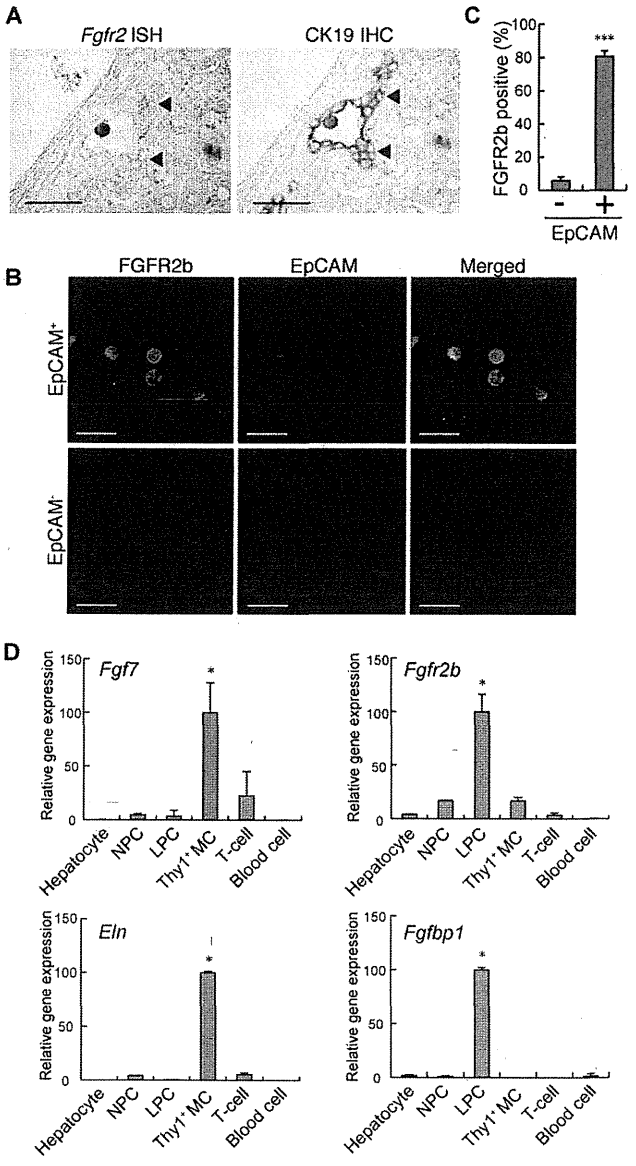


**Figure 2.** FGF7 signal emanates from Thy1$^+$ cells and acts on LPCs. (*A*, *left* panel) Liver sections prepared from mice fed DDC diet for 3 wk were subjected to in situ hybridization analysis for *Fgfr2* expression. (*Right* panel) The same section was subsequently overlaid with immunohistochemical staining using anti-CK19 antibody to confirm its expression in LPCs. Bars, 200 μm. (*B*,*C*) EpCAM$^+$ and EpCAM$^-$ cells were sorted from NPCs in the livers of the mice fed the DDC-containing diet for 5 wk. Cytospin preparations of these cells were stained for FGFR2b (green) and EpCAM (red). Representative images are shown in *B*, and the result of quantitation are shown in *C* (EpCAM$^-$, $n$ = 980; EpCAM$^+$, $n$ = 1454). Mean ± SD. Bars, 40 μm. (***) $P < 0.001$. (*D*) Hepatocyte, NPC, EpCAM$^+$ cell (LPC), Thy1$^+$ CD45$^-$ mesenchymal cell (Thy1$^+$MC), Thy1$^+$ CD45$^+$ T-cell (T-cell), and Thy1$^-$ CD45$^+$ cell (blood cell, excluding T-cell) fractions were isolated from the livers of DDC-treated mice. Expression of the indicated genes was examined by quantitative RT–PCR. Mean ± SD ($n$ = 3). (*) Significantly different from each of the other five fractions (ANOVA, with Tukey post hoc tests, $P < 0.05$).

performed genetic lineage tracing experiments using an *Alfp-Cre* transgenic (Tg) mouse strain, where expression of the Cre recombinase occurred in fetal hepatoblasts and adult hepatocytes and hence enabled us to label and track their descendants. After DDC injury, hepatocytes, BECs, and LPCs were virtually all lineage-labeled. Thy1$^+$ cells, on the other hand, were of a distinct lineage from liver epithelial cells (Supplemental Fig. S4B,C).

FGF-binding protein 1 (FGFBP1) is a soluble protein that can bind a subset of FGFs, including FGF7, and enhance their activities (Beer et al. 2005). Previous studies on skin and renal tube regeneration have shown FGFBP1 to be expressed in epithelial cells rather than mesenchymal cells and to be a target of FGF7 signaling (Liu et al. 2001; Beer et al. 2005). *Fgfbp1* was almost exclusively expressed in LPCs, which further strengthened the notion that LPCs are the primary target of FGF7 signaling from Thy1$^+$ cells (Fig. 2D).

### *Up-regulation of FGF7 is concurrent with expansion of LPCs and Thy1$^+$ cells*

We then examined the correlation of FGF7 with the induction of LPCs and Thy1$^+$ cells in other models of liver injury. First, ligation of the common bile duct (BDL) in mice was used as a model for cholestatic liver disease. FGF7 expression was increased in the BDL-manipulated liver with the LPC response (Fig. 3A,B). As is the case with DDC-induced liver injury, FGF7 in this model was also produced predominantly in Thy1$^+$ cells, while LPCs were the primary target for the signal by expressing the receptor (Supplemental Fig. S5). Second, we checked the activation of LPCs and expression of FGF7 in liver-specific *Tak1*-deficient (*Alfp-Cre*; *Tak1$^{flox/flox}$*, hereafter referred to as *Tak1*-LKO) mice. Loss of *Tak1* in the liver results in chronic inflammation and eventually leads to fibrosis and carcinogenesis (Bettermann et al. 2010; Inokuchi et al. 2010). It is thus considered a faithful model for the progression of human liver diseases. We observed apparent LPC response and expansion of Thy1$^+$ cells in 8-wk-old *Tak1*-LKO mice (Fig. 3C). Concomitantly with the increase of CK19-positive (Fig. 3E) and Thy1-positive (Fig. 3F) areas, the expression of FGF7 was significantly induced (Fig. 3D,G). Although the immunostaining results showed some colocalization of FGF7 with EpCAM$^+$ LPCs, gene expression analysis using isolated cell fractions confirmed that, also in this model, *Fgf7* was mainly produced in Thy1$^+$ cells but not in LPCs (Supplemental Fig. S6). Finally, serum FGF7 levels were found to be increased in human patients with liver diseases such as fulminant hepatic failure and acute hepatitis (Fig. 3H), which often accompany LPC activation. Together, these data suggest that induction of FGF7 upon liver disorders associated with the LPC response is generally conserved in both rodents and humans.

### *FGF7 plays a necessary function as a niche signal for induction of LPCs*

To address the physiological relevance of FGF7 expression in the course of the LPC response, we used *Fgf7*

knockout mice (Guo et al. 1996). They exhibit relatively normal growth and are fertile, with some phenotypes including defects in kidney development, postnatal thymic regeneration, and neurogenesis in the hippocampus (Qiao et al. 1999; Alpdogan et al. 2006; Terauchi et al. 2010; Lee et al. 2012). No liver phenotype during development or in adulthood has been reported. In order to analyze the LPC response in *Fgf7* knockout mice, adult littermates of wild-type and knockout mice were fed a DDC-containing diet or subjected to BDL. We measured the degree of LPC activation by CK19 immunostaining and confirmed that CK19$^+$ LPC numbers were increased by DDC or BDL in the wild-type liver (Fig. 4A,H).

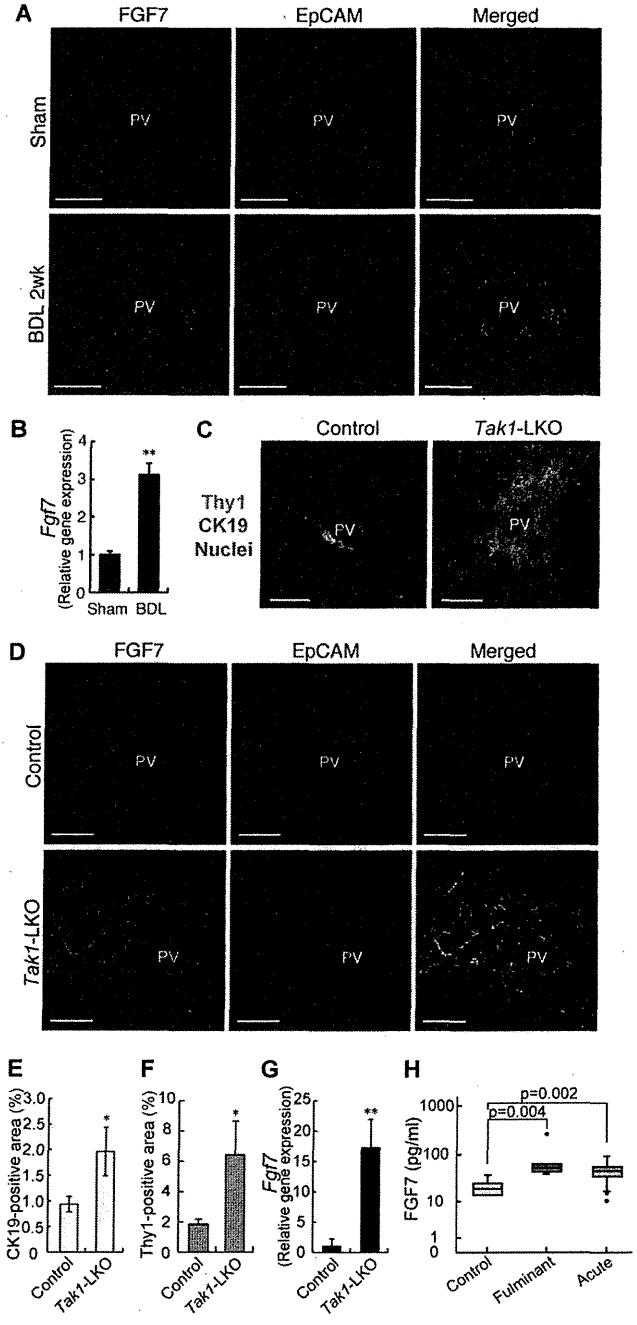


However, the LPC response was almost completely suppressed in *Fgf7* knockout mice (Fig. 4A,B,H,I). In contrast, quantitative analysis of the Thy1$^+$ area in *Fgf7* knockout mice revealed little change when compared with the wild-type control in both normal and damaged livers (Fig. 4C,J). In other words, Thy1$^+$ cells were capable of expanding in response to liver damage even in the absence of FGF7 function, consistent with the notion that FGF7 acts directly on LPCs rather than upstream of Thy1$^+$ cells. Ki67 or TUNEL staining with CK19 revealed that Ki67$^+$ proliferating cells among the CK19$^+$ LPCs were significantly decreased, although not completely abrogated, in the knockout mice compared with the wild-type control, while no statistically significant difference was observed in the TUNEL$^+$ cell population (Supplemental Fig. S7). These results suggest that the suppressed LPC response in *Fgf7* knockout mice can be attributed, at least in part, to reduced proliferation of LPCs rather than augmented induction of their apoptosis.

*Fgf7* knockout mice were highly sensitive to DDC and had a low survival rate, whereas the wild-type mice were more resistant to hepatotoxin-induced liver injury (Fig. 4D). Upon DDC administration, systemic symptoms were obvious and generally more severe in the knockout than in the wild-type control, including jaundice, hemorrhagic diathesis, and weight loss, which are typically observed in end-stage liver disease (Figs. 4E,F; data not shown). Gross pathological and histopathological examinations of the mice that survived at 11 wk of injury confirmed that liver failure with severe leakage of bile into the liver vasculature is the most plausible cause of death in *Fgf7* knockout mice, while no fatal abnormality was recognized in any organs/tissues other than the liver (data not shown). We also performed serum biochemical tests using the mice fed DDC for 10 wk. The cholestasis markers total bilirubin (TBIL) and alkaline phosphatase (ALP) were both

**Figure 3.** FGF7-mediated LPC activation is conserved in several liver injuries. (*A*,*B*) Liver samples prepared from sham-operated (Sham) or BDL mice were subjected to the following experiments. (*A*) Confocal immunofluorescent double staining using anti-FGF7 (green) and anti-EpCAM (red) antibodies. Bars, 50 μm. (PV) Portal vein. (*B*) Quantitative RT–PCR analysis of *Fgf7* mRNA. Mean ± SE ($n$ = 3). (**) $P < 0.01$. (*C*–*G*) Liver samples from 8-wk-old liver-specific *Tak1*-LKO (*Alfp-Cre*; *Tak1*$^{flox/flox}$) or control (*Tak1*$^{flox/flox}$) mice were subjected to the following experiments. (*C*) Representative images for immunofluorescent double staining of CK19 (red) and Thy1 (green). (PV) Portal vein. Bars, 80 μm. (*D*) Confocal immunofluorescent double staining using anti-FGF7 (green) and anti-EpCAM (red) antibodies. Bars, 50 μm. (PV) Portal vein. (*E*) Quantitative image analysis of CK19-positive area. Mean ± SD ($n$ = 3). (*) $P < 0.05$. (*F*) Quantitative image analysis of Thy1-positive area. Mean ± SD ($n$ = 3). (*) $P < 0.05$. (*G*) Quantitative RT–PCR analysis of *Fgf7* mRNA. Mean ± SD ($n$ = 3). (**) $P < 0.01$. (*H*) Serum FGF7 levels in human samples. enzyme-linked immunosorbent assay (ELISA) for human FGF7 was performed on serum samples harvested from healthy controls ($n$ = 6) and patients with fulminant ($n$ = 6) or acute ($n$ = 43) hepatitis. The data are presented as median (25–75 percentile).

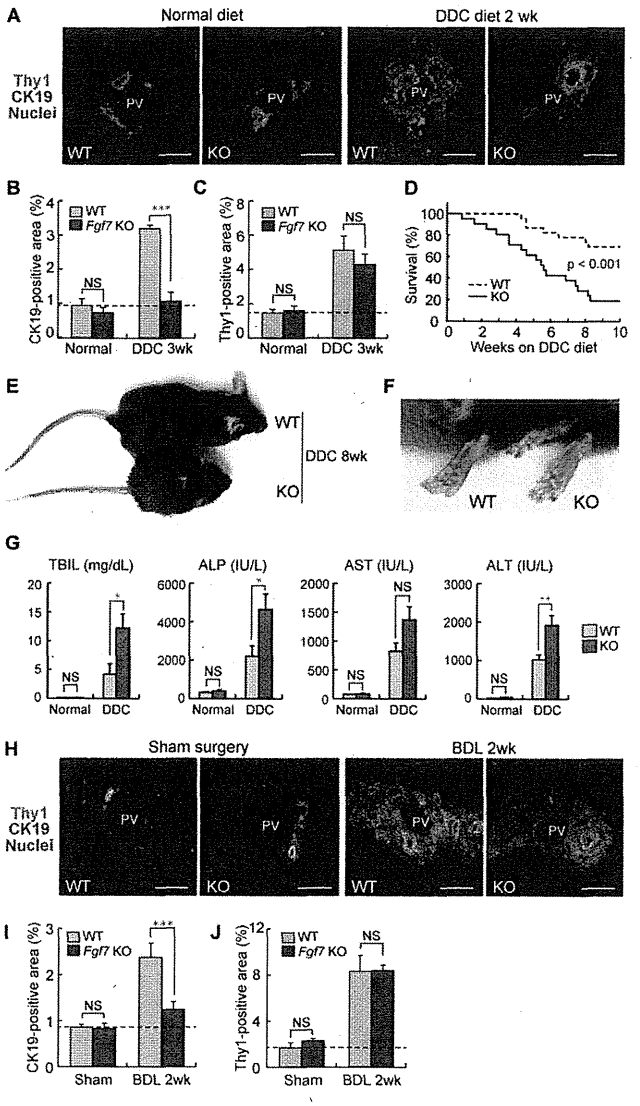


**Figure 4.** FGF7 is essential for LPC activation and liver regeneration in injured livers. Adult littermates of *Fgf7* knockout (KO) and wild-type (WT) mice were fed normal or DDC diet (*A–G*) or subjected to BDL or a sham operation (*H–J*). (*A,H*) Representative images for immunofluorescent double staining of CK19 (red) and Thy1 (green). Bars, 80 μm. (PV) Portal vein. (*B,I*) Quantitative image analysis of CK19-positive area. Mean ± SD ($n = 3$). (***) $P < 0.001$; (NS) not significant. (*C,J*) Quantitative image analysis of Thy1-positive area. Mean ± SD ($n = 3$). (NS) Not significant. (*D*) Kaplan-Meier survival curves of control (wild-type, $n = 23$) and *Fgf7* knockout ($n = 21$) mice given DDC, showing that the lack of FGF7 leads to the increased mortality after DDC feeding. Statistical analysis was performed using the log-rank (Mantel-Cox) test. (*E,F*) Appearance of *Fgf7* knockout and wild-type mice fed DDC diet for 8 wk. (*F*) More severe symptoms for jaundice, such as yellow-colored skin, were typically observed in the knockout animal. (*G*) Serum TBIL, ALP, AST, and ALT levels were measured in control and *Fgf7* knockout mice fed a normal (wild type, $n = 3$; knockout, $n = 3$) or DDC-containing (wild type, $n = 6$; knockout, $n = 3$) diet for 10 wk. Mean ± SE. (**) $P < 0.01$; (*) $P < 0.05$; (NS) not significant.

significantly increased in *Fgf7* knockout mice (Fig. 4G). At the same time, the level of the hepatocyte injury marker alanine transaminase (ALT) was significantly elevated in the knockout mice compared with the wild type, and that of aspartate transaminase (AST) also trended higher, but the difference was not statistically significant (Fig. 4G). At that point, the LPC numbers in the knockout mice could not keep up with those in wild-type mice (Supplemental Fig. S8A–C). These results indicate that the lack of FGF7 exacerbates damages in both hepatocytes and bile ducts and that the LPC response directly correlates with liver function and survival of an organism upon toxic insult. Taken together, we conclude that FGF7 is necessary for LPC activation in vivo at least in two different experimental models, and its expression and function may counter liver dysfunction.

### *Forced expression of FGF7 is sufficient to induce expansion of the LPC population in vivo*

We next performed gain-of-function experiments to further explore the function of FGF7 in regulating the LPC response. First, we examined the effect of FGF7 on LPCs in vitro. We found that a recombinant FGF7 stimulated the proliferation of HSCE1, a cell line derived from $EpCAM^+$ LPCs of adult mice (Okabe et al. 2009), in a dose-dependent manner (Fig. 5A). To examine the effect of FGF7 in vivo, we used *Alfp-Cre; Rosa26-rtTA-IRES-EGFP; tetO-CMV-FGF7* triple Tg mice in which overexpression of FGF7 in the liver is achieved by doxycycline (Dox) treatment (Fig. 5B,C). A significant increase in $CK19^+$ LPC-like cell numbers was observed in the periportal regions of the triple Tg (hereafter referred to as *FGF7* Tg) mouse livers compared with control *Alfp-Cre; Rosa26-rtTA-IRES-EGFP* double Tg mouse livers (Figs. 5D,E). These expanding cells coexpressed other well-known LPC markers: A6, EpCAM, and SOX9 (Fig. 5E; Supplemental Fig. S9A,B). Notably, $A6^+$ $CK19^-$ cells, which can be regarded as a fraction of newly formed hepatocytes (Engelhardt et al. 1990; Ishikawa et al. 2012), were clearly detected adjacent to $A6^+$ $CK19^+$ LPCs in *FGF7* Tg mouse livers as well as in DDC-injured livers (Fig. 5D; Supplemental Fig. S6A), implying that the cell population induced by FGF7 has a potential to differentiate to hepatocytes.

Previous studies have shown that the extracellular matrix (ECM) plays an important role in regulating the LPC response and liver regeneration (Boulter et al. 2012; Español-Suñer et al. 2012). Immunostaining analysis of the type I and type III collagen proteins revealed that there was a significant accumulation of these ECM components around the expanding LPCs in response to FGF7 overexpression, similar to the case observed in the livers of DDC-treated animals (Fig. 5G). This strongly supports the notion that the FGF7-induced LPC induction in the normal liver faithfully recapitulates the phenomenon that occurs under the pathophysiological conditions in diseased livers. Meanwhile, the level of collagen gene expression (*Col1a1* and *Col3a1* for type I and type III collagens, respectively) using the whole-liver mRNA samples showed no significant increase in the expression of

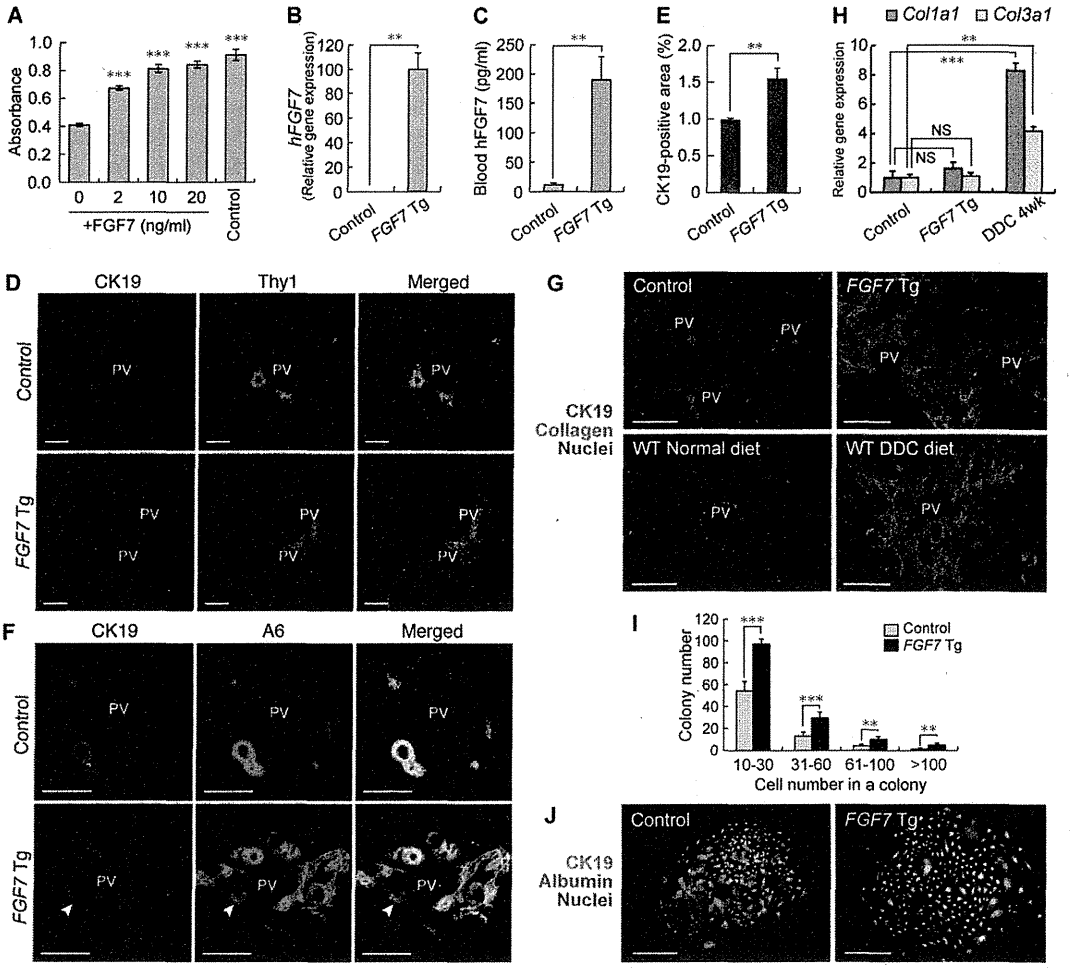


**Figure 5.** Overexpression of FGF7 can induce the LPC response in the adult mouse liver. (*A*) The level of proliferation of HSCE1 cells was examined by WST-1 assay. Stimulation with epidermal growth factor (EGF) and hepatocyte growth factor (HGF) was used as a control. Mean ± SD ($n$ = 3). (***) $P < 0.001$ compared with no cytokine treatment (0). (*B*) Quantitative RT–PCR analysis was performed to assess human *FGF7* mRNA levels in the liver after 3 wk of Dox administration. Mean ± SE (control, $n = 3$; Tg, $n = 5$). (**) $P < 0.01$. (*C*) Serum levels of human FGF7 protein after 3 wk of Dox administration were determined by ELISA. Mean ± SE (control, $n = 4$; Tg, $n = 6$). (**) $P < 0.01$. (*D*) Immunostaining of CK19 (red) and Thy1 (green) in the livers of *FGF7* Tg mice and control mice treated with Dox for 4 wk. Bars, 100 μm. (PV) Portal vein. (*E*) Quantitative analysis of CK19-positive areas showed an increased number of LPC-like cells in *FGF7* Tg mice treated with Dox for 4 wk. Mean ± SD ($n = 3$). (**) $P < 0.01$. (*F*) Immunostaining of CK19 (red) and A6 (green) showed expansion of $CK19^+$ $A6^+$ LPCs in the livers of *FGF7* Tg mice treated with Dox for 4 wk. $CK19^-$ $A6^+$ newly formed hepatocytes were also observed (arrowheads). Bars, 50 μm. (PV) Portal vein. (*G*) Immunostaining of CK19 (red) and collagen (green) in the livers of *FGF7* Tg and control mice, wild-type mice fed a normal diet, and DDC-treated wild-type mice. Bars, 100 μm. (PV) Portal vein. (*H*) Quantitative RT–PCR analysis of *Col1a1* and *Col3a1* mRNA. Mean ± SE (control, $n = 3$; Tg, $n = 5$; DDC, $n = 3$). (**) $P < 0.01$; (***) $P < 0.001$; (NS) not significant. (*I*) $EpCAM^+$ cells were isolated from the livers of *FGF7* Tg mice and control mice 3 wk after Dox treatment and subjected to the in vitro colony formation assay. Mean ± SD ($n = 3$). (**) $P < 0.01$; (***) $P < 0.001$. (*J*) Immunofluorescence images of representative large colonies stained with anti-CK19 (green) and albumin (red). Bars, 200 μm.

either of these genes at the whole-organ level (Fig. 5H). Thus, overexpression of FGF7 in the liver results in local deposition of ECMs associated with the LPC expansion but does not lead to a global fibrogenic response in the organ.

To further characterize the FGF7-induced LPC-like population in terms of functional criteria, we next performed clonogenic assays to evaluate its proliferative and bilineage differentiation potentials in vitro. It has been well documented that stem/progenitor cell activity of a certain population of liver cells can be defined by their capacity to generate large colonies that are capable of expressing both hepatocyte and BEC lineage markers in culture (Suzuki et al. 2008; Okabe et al. 2009; Dorrell et al. 2011; Shin et al. 2011). When $EpCAM^+$ cells isolated from the *FGF7* Tg mice and the control mice were subjected to in vitro colony formation assays (Okabe et al. 2009), the $EpCAM^+$ cells from the Tg mice formed colonies, including those composed of >100 cells (Fig. 5I). Immunostaining analyses confirmed that these large colonies were composed of both albumin-positive (the hepatocyte marker) and CK19-positive (the LPC/BEC marker)

cells, indicative of the bilineage differentiation in vitro (Fig. 5J). Most importantly, the colony-forming rate for both large and smaller colonies was significantly increased in the *FGF7* Tg mice. Thus, overexpression of FGF7 in vivo in the mouse liver leads to expansion of LPCs that are characterized by LPC marker expressions as well as clonogenicity and bipotency in vitro. Taken together, we conclude that FGF7 alone is sufficient to generate a population of cells that are phenotypically and functionally indistinguishable from LPCs.

### *Overexpression of FGF7 reverses both the hepatocyte damage and cholestatic liver injury*

Given the potent activity of FGF7 in promoting the LPC response, we reasoned that application of this molecule should exert some protective effect on the liver against toxic insults. To test this possibility, the Tg mouse system was used to start ectopic FGF7 expression by Dox administration 1 wk after the onset of the course of DDC-induced chronic liver injury (Fig. 6A). Under this condition, increases in the level of the cholestatic markers TBIL and ALP were greatly reduced in *FGF7* Tg mice compared with the control mice, with the severity of symptoms of jaundice being apparently reduced, which means that bile duct obstruction was alleviated (Fig. 6B,C). At the same time, the levels of AST and ALT were also significantly improved in *FGF7* Tg mice, indicating less hepatocyte injury by overexpression of FGF7 (Fig. 6C). To further substantiate the notion that FGF7 does not simply prevent the damage but rather reverses and improves the symptoms of well-established chronic liver failure, we performed similar experiments by starting Dox administration to induce *FGF7* expression in the liver 3 wk after the onset of the DDC administration (Supplemental Fig. S10A,B). Again, serum biochemical analyses showed decreased levels of both hepatocyte injury and cholestasis markers, although the difference was not statistically significant with regard to ALP (Supplemental Fig. S10C). These data suggest that the severity of the damage on both hepatocytes and BECs can be relieved by an excess of FGF7 through the activation of LPCs that are bipotential and hence capable of contributing to the recovery of both lineages.

Histochemical examination revealed that deposition of brown pigment plugs derived from porphyrin crystals, a hallmark of the DDC-injured liver, was decreased in the Tg liver (Fig. 6D). Single-cell necrosis was reduced in

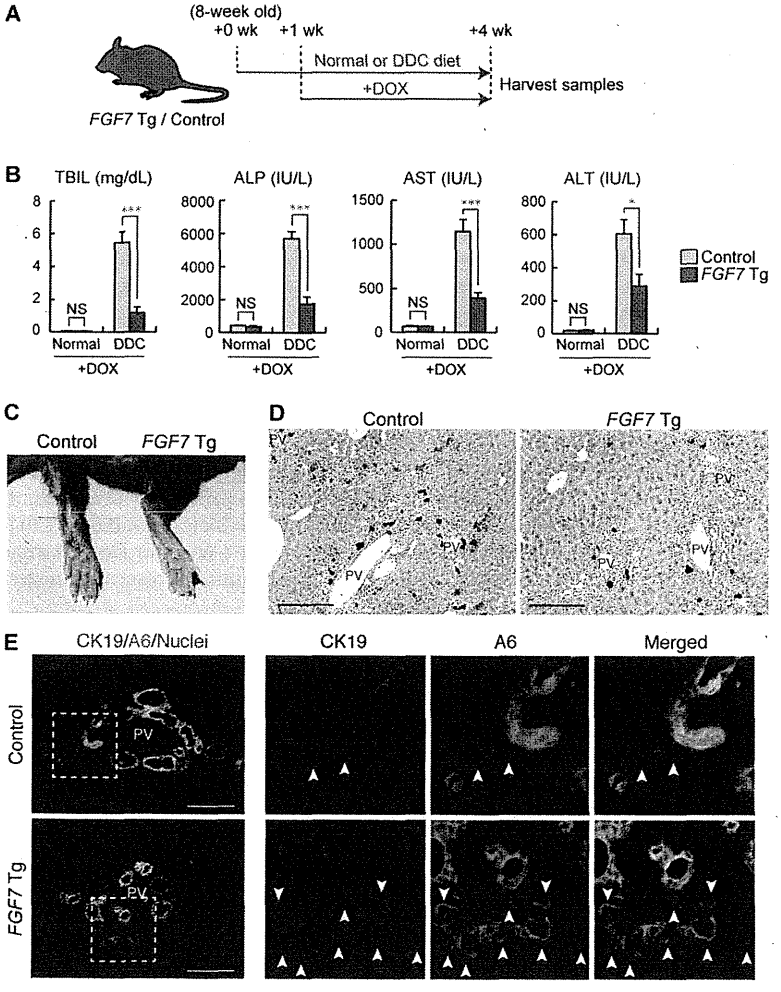


**Figure 6.** Application of FGF7 improves both the hepatocyte damage and cholestatic liver injury. (*A*) Schematic representation of the experiment. Eight-week-old *FGF7* Tg and control mice were subjected to the DDC-induced liver injury model or left untreated, and 1 wk later, Dox administration was started for FGF7 induction. After 3 wk of treatment, serum and liver samples were harvested for subsequent analyses. (*B*) Serum TBIL, ALP, AST, and ALT levels were measured in control and *FGF7* Tg mice fed a normal (control, $n = 3$; Tg, $n = 3$) or DDC-containing (control, $n = 9$; Tg, $n = 7$) diet. Mean ± SE. (***) $P < 0.001$; (*) $P < 0.05$; (NS) not significant. (*C*) Typical skin color (*right* foot) of the DDC-treated animals at the end of the protocol, indicating that *FGF7* Tg mice suffered less from jaundice than control mice. (*D*) Hematoxylin and eosin staining of livers from DDC-treated animals at the end of the protocol. Bars, 200 μm. (PV) Portal vein. (*E*) Immunostaining of CK19 (red) and A6 (green) in the livers of FGF7 Tg mice and control mice at the end of the protocol. Note that $A6^+$ $CK19^-$ newly formed hepatocytes were increased in the livers of *FGF7* Tg mice. Bars, 100 μm. (PV) Portal vein.

some of the Tg mice compared with the control (data not shown). In the case of the mice fed DDC for 6 wk, some morphological changes associated with the reacting ductules were observed in the Tg mice, including thickened epithelial layers and more dilated luminal structures (Supplemental Fig. S10D,E). Most remarkably, immunostaining analyses revealed that A6$^+$ CK19$^-$ newly formed hepatocytes were dramatically increased around the expanding A6$^+$ CK19$^+$ LPCs (Figs. 6E; Supplemental Fig. S10E). This strongly suggests that overexpression of FGF7 contributes to parenchymal regeneration by accelerating differentiation and production of hepatocytes from LPCs in the DDC-induced liver injury model. In conclusion, our results indicate that FGF7 secreted by Thy1$^+$ cells mediates the activation of adult LPCs as a niche signal and promotes progenitor cell-dependent liver regeneration (Fig. 7).

## Discussion

In this study, we demonstrate that FGF7 plays a critical role in inducing LPCs and that the LPC response contributes to survival in severe liver injury. From the standpoint of adult tissue stem/progenitor cells, this study has substantiated the concept of the niche for LPCs in the regenerating liver by molecular characterization.

In general, tissue stem/progenitor cells are supported and regulated by their surrounding microenvironment or the stem cell niche. While several secreted molecules that participate in the LPC response have been reported (Erker and Grompe 2007), their possible involvement as niche signals has not been explored. This study provides compelling evidence that Thy1$^+$ periportal cells form the niche for LPCs by residing in close proximity to LPCs and producing a key regulatory factor, FGF7. Since FGF7-producing Thy1$^+$ cells express markers for portal fibroblasts, hepatic stellate cells, and myofibroblast, we consider that Thy1$^+$ cells are a heterogeneous population of mesenchymal cells. Our data are consistent with a previous report that hepatic stellate cells express FGF7 in chronic liver disease (Steiling et al. 2004). Although further characterization of the Thy1$^+$ cells is needed to give a clear definition of the LPC niche, we hereby propose that the stem cell niche is present in the adult liver under the regenerating conditions. It has been reported that Thy1$^+$ cells are also observed in the livers of patients with fulminant liver failure accompanying the LPC response (Dezso et al. 2007). In addition, high expression of FGF7 in patients with chronic liver diseases (Steiling et al. 2004; Otte et al. 2007) and in experimental rat models of hepatic fibrosis (Murakami et al. 2011) were previously reported. Thus, we predict that LPCs are regulated through the same mechanism in humans as in rodents.

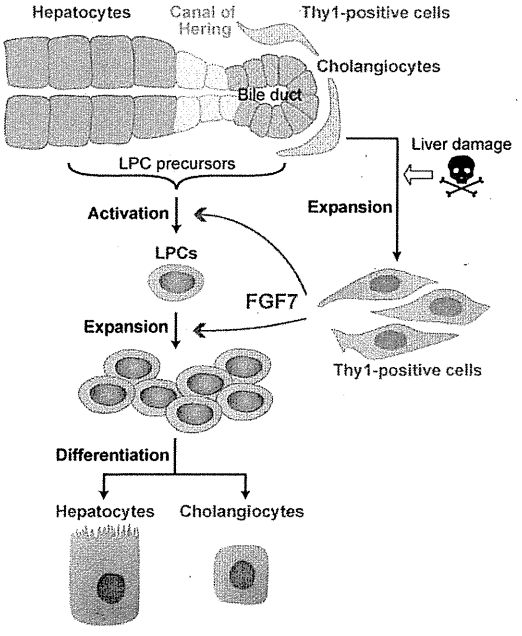


**Figure 7.** A model for regulatory mechanism of the LPC response by FGF7. In injured livers, Thy1$^+$ mesenchymal cells expand in the periportal area and produce FGF7. FGF7 contributes to liver regeneration by initiating the activation and proliferation of LPCs as the functional niche signal.

The LPC response is a complicated physiological response to liver injuries involving several kinds of cells, such as hepatocytes, BECs, immune cells, hepatic stellate cells, and portal fibroblasts. We demonstrated that FGF7 is both necessary and sufficient for its induction. To our knowledge, this is the first study to prove that FGF signaling is involved in LPC regulation. Upstream and downstream signaling events of FGF7 need to be explored to further elucidate the regulatory mechanism of LPCs. Previous studies have identified TNF (tumor necrosis factor)-like weak inducer of apoptosis (Tweak) as a mitogen for LPCs (Jakubowski et al. 2005; Tirnitz-Parker et al. 2010). Tweak is a member of the TNF family and binds to the FGF-inducible 14-kDa protein (Fn14) receptor (Meighan-Mantha et al. 1999). Although the LPC response in *Fn14* knockout mice was attenuated after 2 wk of CDE treatment, it was restored later and eventually resulted in a level equivalent to that in wild-type mice (Tirnitz-Parker et al. 2010). In contrast, we showed in this study that LPC activation was not sufficiently induced in *Fgf7* knockout mice even after long-term liver injury. Thus, the role of FGF7 signal may be more direct and indispensable in LPC induction, while that of the Tweak/Fn14 pathway may be rather enhancing and not necessarily required. Recently, hepatocyte growth factor (HGF)/c-Met signaling has been reported to play a necessary role in LPC-mediated liver regeneration in the mouse DDC diet model (Ishikawa et al. 2012), although it remains unexplored whether it can also be sufficient to induce the LPC response, as is the case with FGF7. The relationship between FGF7 and these signaling pathways is an important issue to be addressed. In addition, recent studies have suggested that the cellular and molecular mechanisms underlying the injury/regeneration processes in the DDC injury are apparently different from the CDE regimen, another well-appreciated model to study LPCs (Boulter et al. 2012; Español-Suñer et al. 2012). It should be determined whether and how FGF7 is involved in the latter case.

We showed that forced expression of FGF7 in hepatocytes induces the LPC response in the normal liver. Intriguingly, induced LPC-like cells were observed only in the periportal area despite global expression of FGF7 within the liver. As the LPC response upon liver injury also takes place in the periportal region, FGF7-induced LPC-like cells may be derived from the genuine origin and undergo the normal ontogeny of LPCs. The origin of LPCs is still under debate. The canals of Hering that connect bile ducts to hepatocytes have long been considered a promising candidate (Paku et al. 2001); however, direct proof of this idea has been hampered by the lack of a specific molecular marker for these cells. BECs are phenotypically quite similar to LPCs and can thus be a likely candidate (Alison et al. 1996; Okabe et al. 2009). Indeed, recent studies using a genetic lineage tracing system based on *Sox9-CreERT2* mouse lines have suggested this possibility (Dorrell et al. 2011; Furuyama et al. 2011), although the nature of the Sox9-expressing cells should be further evaluated and rigorously determined with considerable caution (Carpentier et al. 2011). At the same time, hepatocytes have also been considered as possible LPC precursors, as they can be converted to BEC- or LPC-like cells under certain circumstances (Michalopoulos et al. 2005; Nishikawa et al. 2005; Zong et al. 2009). With regard to this notion, it should be noted that while FGFR2b is highly expressed in LPCs, it is also weakly but certainly expressed in the hepatocyte fraction. Considering the heterogeneity of hepatocytes, it is worthwhile to explore the nature of LPC precursors based on the expression pattern of FGFR2b. It is also possible that the local environmental cues, such as ECMs, in the periportal region participate in dictating the competence of LPC precursors for activation by FGF7, leading to a spatially stereotyped induction pattern of the LPC response.

While it has long been documented that LPCs appear and proliferate in injured and cancerous livers, whether LPCs participate in regeneration has not been clear to date. Our data, based on loss-of-function and gain-of-function experiments with FGF7, demonstrate that the level of LPC activation correlates with resilience and survival in cases of severe liver injury and suggest that LPCs practically contribute to liver regeneration. It is formally not excluded that FGF7 may act directly on damaged hepatocytes and/or BECs to cause some protective effects, and further analyses will be required to discriminate these possibilities. In either case, FGF7 can be regarded as a highly effective molecule to reverse liver damage. It has been reported that application of recombinant FGF7 protein in mice results in enhanced expression of detoxifying enzymes in the liver, while mice lacking both FGFR1 and FGFR2 in hepatocytes show increased mortality after PHx with impaired expression of those enzymes (Böhm et al. 2010). PHx has generally been regarded as the model for liver regeneration achieved by compensatory proliferation of hepatocytes rather than by LPCs, but several recent studies have implicated a possible involvement of the latter as well (Furuyama et al. 2011; Iverson et al. 2011; Malato et al. 2011). Although the study by Böhm et al. (2010) did not mean to address the role of endogenous FGF7, it would be worth exploring whether the potential beneficial effect of FGF7 observed therein is attributable to ectopic activation of LPCs. An N-terminally truncated form of FGF7, palifermin, has already been approved for the treatment of chemoradiation-induced oral mucositis (Beaven and Shea 2007). In spite of the ability of this drug to improve wound healing responses, its potential for therapeutic application to human liver diseases has not been tested. Our present study provides evidence that FGF7 or its derivatives may have clinical implications for patients with hepatic dysfunction as well.

## Materials and methods

### *Animals*

*Fgf7* knockout mice (Guo et al. 1996) were obtained from The Jackson Laboratory. All of the experiments in this study were performed on littermates derived from the mating of heterozygotes. In order to generate liver-specific *Tak1*-deficient mice (*Tak1*-LKO mice), mice carrying floxed alleles of the *Tak1* gene ($Tak1^{flox/flox}$) (Sato et al. 2005), maintained by and obtained from JCRB (Japanese Collection of Research Bioresources Cell Bank) Laboratory Animal Resource Bank, NIBIO (National Institute of Biomedical Innovation, Osaka), were crossed with *Alfp-Cre* Tg mice (kindly provided by Dr. Klaus Kaestner, University of Pennsylvania) (Zhang et al. 2005). For the *FGF7* Tg mouse line in which human FGF7 is overexpressed in the liver upon treatment with Dox, the *Alfp-Cre* Tg mice, *ROSA26-rtTA-IRES-EGFP* knock-in mice (obtained from The Jackson Laboratory) (Belteki et al. 2005), and *tetO-CMV-FGF7* Tg mice (kindly provided by Dr. Jeffrey A. Whitsett, Cincinnati Children's Hospital Medical Center) (Tichelaar et al. 2000) were crossed to prepare *Alfp-Cre; rtTA/+; FGF7* triple Tg mice. Littermates lacking the *FGF7* transgene (*Alfp-Cre; rtTA/+*) were used as a control. Dox was administrated in drinking water (2 g/L) supplemented with 1% sucrose. For lineage tracing experiments, the *Alfp-Cre* Tg mice were crossed with the *R26R-EYFP* reporter strain (Srinivas et al. 2001). Wild-type C57BL/6J mice were purchased from CLEA Japan, Inc. All animals were maintained under standard SPF conditions. The experiments were performed according to the guideline set by the institutional animal care and use committee of the University of Tokyo. Mouse LPCs were activated by feeding with a 0.1% DDC-containing diet (F-4643, Bio-serv) or common BDL using a standard technique.

### *Antibodies*

For immunohistochemistry, rat monoclonal antibodies against mouse EpCAM (used at a dilution of 1:200; 552370) and Thy1 (1:200; 553011) were purchased from BD Bioscience. The goat anti-mouse albumin (1:100; A90-234A, Bethyl Laboratories), rabbit anti-Desmin (1:400; ab8592, Abcam), rabbit anti-rat Elastin (1:100; CL55041AP, Cedarlane), rabbit anti-GFP (1:50; G10362, Life Technologies), rabbit anti-human Ki67 (1:200; NCL-Ki67p, Leica), and rabbit anti-Sox9 (1:1000; AB5535, Millipore) antibodies were also commercially obtained and used. A mixture of rabbit anti-collagen type I (1:100; 2150-1410, AbD serotec) and rabbit anti-collagen type III (1:300; ab7778, Abcam) was used to detect collagen fibers. The rat anti-mouse CK19 (TROMA-III) was obtained from the Developmental Studies Hybridoma Bank and used at 250 ng/mL. The rabbit anti-mouse CK19 antibody (1:1000–1:2000) was raised as previously described (Tanimizu

et al. 2003). The rabbit anti-FGF7 (1:100) and anti-FGFR2b (1:200) antibodies were as described (Yamamoto-Fukuda et al. 2003). The A6 antibody (1:10–1:20) was a generous gift from Dr. Valentina Factor (National Institutes of Health). For flow cytometry, the rat anti-EpCAM monoclonal antibody (1:500) was raised as described previously (Okabe et al. 2009). The rat anti-mouse CD45 APC antibody (1:100; 30-F11) was purchased from BD Bioscience. The anti-Thy1 antibody was the same as described above.

*Histological analysis*

Frozen sections (8 μm) from the liver were placed on APS-coated glass slides (Matsunami Glass) using a HM505E cryostat (Microm International). After blocking in 5% skim milk/PBS, the samples were incubated with primary antibodies and then with fluorescence-conjugated secondary antibodies. Nuclei were counterstained with Hoechst 33342 (Sigma). Liver sections were imaged with fluorescence microscopes (Axioskop 2 plus and Axio Observer.Z1, Zeiss) or a confocal microscope (Fluoview FV1000, Olympus). For the quantification of positive areas, immunostained liver sections were imaged and quantified using an In Cell Analyzer 2000 (GE Healthcare). TUNEL assay was performed using the In Situ Apoptosis Detection kit (MK500, TaKaRa) according to the manufacturer's instructions. Gross pathological and histopathological examinations of *Fgf7* knockout and control mice were performed by BOZO Research Center, Inc.

*Section in situ hybridization analysis*

Paraffin sections were prepared from liver specimens, and a digoxigenin-labeled antisense RNA probe for mouse *Fgfr2* was used for in situ hybridization by the method of Genostaff, Inc. The probe sequence is shown in Supplemental Table S2, and the hybridization conditions are available on request. After images for in situ hybridization staining were obtained, the sections were further processed for immunohistochemical staining with the anti-CK19 antibody. The same fields of view as in in situ hybridization were chosen and photographed.

*Cell preparation and flow cytometry*

A single-cell suspension from the liver was obtained by a two-step collagenase perfusion method as described previously (Okabe et al. 2009). In short, liver specimens were perfused with basic perfusion solution containing 0.5 g/L collagenase type IV (Sigma). The undigested clot was redigested with basic perfusion solution containing 0.5 g/L collagenase type IV, 0.5 g/L pronase (Roche), and 50 mg/L DNaseI (Sigma). This digested liver was passed through a 70-μm cell strainer. After centrifugation at 700 rpm for 2 min, the pellet was used for separation of hepatocytes by Percoll density centrifugation. The supernatant was transferred to a new tube and centrifuged repeatedly until no pellet was visible. The final supernatant was centrifuged at 1200 rpm for 5 min, and the precipitated cells were used as NPCs for flow cytometry. Aliquots of cells were blocked with anti-FcR antibody, costained with fluorescence- and/or biotin-conjugated antibodies, and then incubated with PE-conjugated streptavidin (BD Biosciences) if needed. The samples were analyzed by FACSCalibur (Becton Dickinson) or sorted by Moflo XDP (Beckman-Coulter). Dead cells were excluded by propidium iodide staining.

*Quantitative RT–PCR*

Total RNA was isolated from whole-liver samples or sorted cell populations using Trizol reagent (Invitrogen) and treated with DNaseI (Invitrogen). Total RNA and random hexamer primers were used for cDNA synthesis with SuperScript III (Invitrogen) or High-Capacity cDNA Reverse Transcription kit (Applied Biosystems). Quantitative RT–PCR analyses were performed using LightCycler (Roche) with SYBR Premix Ex Taq (Takara). *Gapdh* was used as an internal control. Primer sequences are listed in Supplemental Table S1.

*Cell culture and proliferation assay*

The hepatic progenitor cell line HSCE1 was established and characterized as described previously (Okabe et al. 2009). HSCE1 cells were maintained in type I collagen-coated dishes using a medium supplemented with fetal bovine serum and 10 ng/mL each recombinant human EGF and HGF. The proliferative response of HSCE1 cells was examined in the absence of the serum by a colorimetric assay using WST-1 cell proliferation reagent (Roche) according to the manufacturer's directions. The absorbance value (OD450-OD650) was measured using an Emax microplate reader (Molecular Devices).

*In vitro colony formation assay*

$EpCAM^+$ cells were sorted as described previously (Okabe et al. 2009) and plated at $5 \times 10^3$ cells per 35-mm dish. The cells were cultured for 9 d, and then the number and size of colonies were counted.

*Human FGF7 immunoassay*

Human FGF7 concentration in serum was quantitatively determined in duplicate by FGF7-specific enzyme-linked immunosorbent assay (ELISA; R&D systems, Inc.) according to the manufacturer's instructions. In brief, FGF7 standards and samples were placed in the provided monoclonal antibody-coated microplates. After the reaction, an enzyme-linked polyclonal antibody specific for FGF7 was added and incubated for 2 h at room temperature. The unbound components were washed off at each step, whereas bound FGF7 was determined by ELISA reader (Immunomini NJ2300, Cosmo Bio Co., Ltd.). Statistical analysis in Figure 3H was carried out using a Kruskal-Wallis test and a Mann-Whitney test in SPSS Statistics 17.0 software. The study protocol conformed to the ethical guidelines of the 1975 Declaration of Helsinki and was approved by the ethics committees of Iwate Medical University and The University of Tokyo. Informed consent was obtained from all patients.

*Statistical analysis*

Data were analyzed and statistics were performed using unpaired two-tailed Student's *t*-test unless otherwise indicated. Comparisons of gene expression in multiple liver cell fractions (Fig. 2D; Supplemental Figs. S4A, S5, S6) were done using one-way analysis of variance (ANOVA) with subsequent Tukey tests. $P < 0.05$ was considered statistically significant.

## Acknowledgments

We thank Dr. K. Kaestner, Dr. J.A. Whitsett, and JCRB Laboratory Animal Resource Bank at NIBIO for providing mouse strains; Dr. V. Factor for an antibody; H. Bae, Y. Kamiya, A. Kikuchi, N. Miyata, S. Saito, and H. Sato for technical assistance; and the members of the Miyajima laboratory for discussions and suggestions. The TROMA-III developed by Dr. Rolf Kemler was obtained from the Developmental Studies Hybridoma Bank developed under the auspices of the NICHD and maintained by the Department of Biology at The University of Iowa. This

work was supported by research grants from the Ministry of Education, Culture, Sports, Science, and Technology of Japan (to T.I. and A.M.); Ministry of Health, Labor, and Welfare of Japan (to A.M.); the CREST program from Japan Science and Technology Agency (to A.M.); and the Takeda Science Foundation (to A.M.). H.M.T. was a Research Fellow of the Japan Society for the Promotion of Science.

## References

Akhurst B, Croager EJ, Farley-Roche CA, Ong JK, Dumble ML, Knight B, Yeoh GC. 2001. A modified choline-deficient, ethionine-supplemented diet protocol effectively induces oval cells in mouse liver. *Hepatology* **34:** 519–522.

Alison MR, Golding MH, Sarraf CE. 1996. Pluripotential liver stem cells: Facultative stem cells located in the biliary tree. *Cell Prolif* **29:** 373–402.

Alpdogan O, Hubbard VM, Smith OM, Patel N, Lu S, Goldberg GL, Gray DH, Feinman J, Kochman AA, Eng JM, et al. 2006. Keratinocyte growth factor (KGF) is required for postnatal thymic regeneration. *Blood* **107:** 2453–2460.

Beaven AW, Shea TC. 2007. The effect of palifermin on chemotherapyand radiation therapy-induced mucositis: A review of the current literature. *Support Cancer Ther* **4:** 188–197.

Beer HD, Bittner M, Niklaus G, Munding C, Max N, Goppelt A, Werner S. 2005. The fibroblast growth factor binding protein is a novel interaction partner of FGF-7, FGF-10 and FGF-22 and regulates FGF activity: Implications for epithelial repair. *Oncogene* **24:** 5269–5277.

Belteki G, Haigh J, Kabacs N, Haigh K, Sison K, Costantini F, Whitsett J, Quaggin SE, Nagy A. 2005. Conditional and inducible transgene expression in mice through the combinatorial use of Cre-mediated recombination and tetracycline induction. *Nucleic Acids Res* **33:** e51.

Bettermann K, Vucur M, Haybaeck J, Koppe C, Janssen J, Heymann F, Weber A, Weiskirchen R, Liedtke C, Gassler N, et al. 2010. TAK1 suppresses a NEMO-dependent but NF-κB-independent pathway to liver cancer. *Cancer Cell* **17:** 481–496.

Bird TG, Lorenzini S, Forbes SJ. 2008. Activation of stem cells in hepatic diseases. *Cell Tissue Res* **331:** 283–300.

Böhm F, Speicher T, Hellerbrand C, Dickson C, Partanen JM, Ornitz DM, Werner S. 2010. FGF receptors 1 and 2 control chemically induced injury and compound detoxification in regenerating livers of mice. *Gastroenterology* **139:** 1385–1396.

Boulter L, Govaere O, Bird TG, Radulescu S, Ramachandran P, Pellicoro A, Ridgway RA, Seo SS, Spee B, Van Rooijen N, et al. 2012. Macrophage-derived Wnt opposes Notch signaling to specify hepatic progenitor cell fate in chronic liver disease. *Nat Med* **18:** 572–579.

Carpentier R, Suñer RE, van Hul N, Kopp JL, Beaudry JB, Cordi S, Antoniou A, Raynaud P, Lepreux S, Jacquemin P, et al. 2011. Embryonic ductal plate cells give rise to cholangiocytes, periportal hepatocytes, and adult liver progenitor cells. *Gastroenterology* **141:** 1432–1438.

Dezso K, Jelnes P, Laszlo V, Baghy K, Bodor C, Paku S, Tygstrup N, Bisgaard HC, Nagy P. 2007. Thy-1 is expressed in hepatic myofibroblasts and not oval cells in stem cell-mediated liver regeneration. *Am J Pathol* **171:** 1529–1537.

Dorrell C, Erker L, Schug J, Kopp JL, Canaday PS, Fox AJ, Smirnova O, Duncan AW, Finegold MJ, Sander M, et al. 2011. Prospective isolation of a bipotential clonogenic liver progenitor cell in adult mice. *Genes Dev* **25:** 1193–1203.

Duncan AW, Dorrell C, Grompe M. 2009. Stem cells and liver regeneration. *Gastroenterology* **137:** 466–481.

Engelhardt NV, Factor VM, Yasova AK, Poltoranina VS, Baranov VN, Lasareva MN. 1990. Common antigens of mouse oval and biliary epithelial cells. Expression on newly formed hepatocytes. *Differentiation* **45:** 29–37.

Erker L, Grompe M. 2007. Signaling networks in hepatic oval cell activation. *Stem Cell Res* **1:** 90–102.

Español-Suñer R, Carpentier R, Van Hul N, Legry V, Achouri Y, Cordi S, Jacquemin P, Lemaigre F, Leclercq IA. 2012. Liver progenitor cells yield functional hepatocytes in response to chronic liver injury in mice. *Gastroenterology* **143:** 1564–1575.

Farber E. 1956. Similarities in the sequence of early histological changes induced in the liver of the rat by ethionine, 2-acetylamino-fluorene, and 3′-methyl-4-dimethylaminoazobenzene. *Cancer Res* **16:** 142–148.

Fausto N. 2004. Liver regeneration and repair: Hepatocytes, progenitor cells, and stem cells. *Hepatology* **39:** 1477–1487.

Furuyama K, Kawaguchi Y, Akiyama H, Horiguchi M, Kodama S, Kuhara T, Hosokawa S, Elbahrawy A, Soeda T, Koizumi M, et al. 2011. Continuous cell supply from a Sox9-expressing progenitor zone in adult liver, exocrine pancreas and intestine. *Nat Genet* **43:** 34–41.

Gerhart J. 1999. 1998 Warkany lecture: Signaling pathways in development. *Teratology* **60:** 226–239.

Guo L, Degenstein L, Fuchs E. 1996. Keratinocyte growth factor is required for hair development but not for wound healing. *Genes Dev* **10:** 165–175.

Inokuchi S, Aoyama T, Miura K, Osterreicher CH, Kodama Y, Miyai K, Akira S, Brenner DA, Seki E. 2010. Disruption of TAK1 in hepatocytes causes hepatic injury, inflammation, fibrosis, and carcinogenesis. *Proc Natl Acad Sci* **107:** 844–849.

Ishikawa T, Factor VM, Marquardt JU, Raggi C, Seo D, Kitade M, Conner EA, Thorgeirsson SS. 2012. Hepatocyte growth factor/c-met signaling is required for stem-cell-mediated liver regeneration in mice. *Hepatology* **55:** 1215–1226.

Itoh N, Ornitz DM. 2008. Functional evolutionary history of the mouse Fgf gene family. *Dev Dyn* **237:** 18–27.

Iverson SV, Comstock KM, Kundert JA, Schmidt EE. 2011. Contributions of new hepatocyte lineages to liver growth, maintenance, and regeneration in mice. *Hepatology* **54:** 655–663.

Jakubowski A, Ambrose C, Parr M, Lincecum JM, Wang MZ, Zheng TS, Browning B, Michaelson JS, Baetscher M, Wang B, et al. 2005. TWEAK induces liver progenitor cell proliferation. *J Clin Invest* **115:** 2330–2340.

Knight B, Matthews VB, Olynyk JK, Yeoh GC. 2005. Jekyll and Hyde: Evolving perspectives on the function and potential of the adult liver progenitor (oval) cell. *Bioessays* **27:** 1192–1202.

Knight B, Akhurst B, Matthews VB, Ruddell RG, Ramm GA, Abraham LJ, Olynyk JK, Yeoh GC. 2007. Attenuated liver progenitor (oval) cell and fibrogenic responses to the choline deficient, ethionine supplemented diet in the BALB/c inbred strain of mice. *J Hepatol* **46:** 134–141.

Lee CH, Javed D, Althaus AL, Parent JM, Umemori H. 2012. Neurogenesis is enhanced and mossy fiber sprouting arises in FGF7-deficient mice during development. *Mol Cell Neurosci* **51:** 61–67.

Libbrecht L, Roskams T. 2002. Hepatic progenitor cells in human liver diseases. *Semin Cell Dev Biol* **13:** 389–396.

Liu XH, Aigner A, Wellstein A, Ray PE. 2001. Up-regulation of a fibroblast growth factor binding protein in children with renal diseases. *Kidney Int* **59:** 1717–1728.

Lowes KN, Brennan BA, Yeoh GC, Olynyk JK. 1999. Oval cell numbers in human chronic liver diseases are directly related to disease severity. *Am J Pathol* **154:** 537–541.

Lu J, Izvolsky KI, Qian J, Cardoso WV. 2005. Identification of FGF10 targets in the embryonic lung epithelium during bud morphogenesis. *J Biol Chem* **280:** 4834–4841.

Malato Y, Naqvi S, Schürmann N, Ng R, Wang B, Zape J, Kay MA, Grimm D, Willenbring H. 2011. Fate tracing of mature hepatocytes in mouse liver homeostasis and regeneration. *J Clin Invest* **121:** 4850–4860.

Meighan-Mantha RL, Hsu DK, Guo Y, Brown SA, Feng SL, Peifley KA, Alberts GF, Copeland NG, Gilbert DJ, Jenkins NA, et al. 1999. The mitogen-inducible Fn14 gene encodes a type I transmembrane protein that modulates fibroblast adhesion and migration. *J Biol Chem* **274:** 33166–33176.

Michalopoulos GK, DeFrances MC. 1997. Liver regeneration. *Science* **276:** 60–66.

Michalopoulos GK, Barua L, Bowen WC. 2005. Transdifferentiation of rat hepatocytes into biliary cells after bile duct ligation and toxic biliary injury. *Hepatology* **41:** 535–544.

Murakami KI, Kaji T, Shimono R, Hayashida Y, Matsufuji H, Tsuyama S, Maezono R, Kosai KI, Takamatsu H. 2011. Therapeutic effects of vitamin A on experimental cholestatic rats with hepatic fibrosis. *Pediatr Surg Int* **27:** 863–870.

Nishikawa Y, Doi Y, Watanabe H, Tokairin T, Omori Y, Su M, Yoshioka T, Enomoto K. 2005. Transdifferentiation of mature rat hepatocytes into bile duct-like cells in vitro. *Am J Pathol* **166:** 1077–1088.

Okabe M, Tsukahara Y, Tanaka M, Suzuki K, Saito S, Kamiya Y, Tsujimura T, Nakamura K, Miyajima A. 2009. Potential hepatic stem cells reside in $EpCAM^+$ cells of normal and injured mouse liver. *Development* **136:** 1951–1960.

Otte JM, Schwenger M, Brunke G, Schmitz F, Otte C, Kiehne K, Kloehn S, Monig H, Schmidt WE, Herzig KH. 2007. Differential regulated expression of keratinocyte growth factor and its receptor in experimental and human liver fibrosis. *Regul Pept* **144:** 82–90.

Paku S, Schnur J, Nagy P, Thorgeirsson SS. 2001. Origin and structural evolution of the early proliferating oval cells in rat liver. *Am J Pathol* **158:** 1313–1323.

Ponder KP. 1996. Analysis of liver development, regeneration, and carcinogenesis by genetic marking studies. *FASEB J* **10:** 673–682.

Preisegger KH, Factor VM, Fuchsbichler A, Stumptner C, Denk H, Thorgeirsson SS. 1999. Atypical ductular proliferation and its inhibition by transforming growth factor β1 in the 3,5-diethoxycarbonyl-1,4-dihydrocollidine mouse model for chronic alcoholic liver disease. *Lab Invest* **79:** 103–109.

Qiao J, Uzzo R, Obara-Ishihara T, Degenstein L, Fuchs E, Herzlinger D. 1999. FGF-7 modulates ureteric bud growth and nephron number in the developing kidney. *Development* **126:** 547–554.

Sato S, Sanjo H, Takeda K, Ninomiya-Tsuji J, Yamamoto M, Kawai T, Matsumoto K, Takeuchi O, Akira S. 2005. Essential function for the kinase TAK1 in innate and adaptive immune responses. *Nat Immunol* **6:** 1087–1095.

Shin S, Walton G, Aoki R, Brondell K, Schug J, Fox A, Smirnova O, Dorrell C, Erker L, Chu AS, et al. 2011. Foxl1-Cre-marked adult hepatic progenitors have clonogenic and bilineage differentiation potential. *Genes Dev* **25:** 1185–1192.

Srinivas S, Watanabe T, Lin CS, William CM, Tanabe Y, Jessell TM, Costantini F. 2001. Cre reporter strains produced by targeted insertion of EYFP and ECFP into the ROSA26 locus. *BMC Dev Biol* **1:** 4.

Steiling H, Werner S. 2003. Fibroblast growth factors: Key players in epithelial morphogenesis, repair and cytoprotection. *Curr Opin Biotechnol* **14:** 533–537.

Steiling H, Muhlbauer M, Bataille F, Scholmerich J, Werner S, Hellerbrand C. 2004. Activated hepatic stellate cells express keratinocyte growth factor in chronic liver disease. *Am J Pathol* **165:** 1233–1241.

Strick-Marchand H, Masse GX, Weiss MC, Di Santo JP. 2008. Lymphocytes support oval cell-dependent liver regeneration. *J Immunol* **181:** 2764–2771.

Suzuki A, Sekiya S, Onishi M, Oshima N, Kiyonari H, Nakauchi H, Taniguchi H. 2008. Flow cytometric isolation and clonal identification of self-renewing bipotent hepatic progenitor cells in adult mouse liver. *Hepatology* **48:** 1964–1978.

Tanimizu N, Miyajima A. 2007. Molecular mechanism of liver development and regeneration. *Int Rev Cytol* **259:** 1–48.

Tanimizu N, Nishikawa M, Saito H, Tsujimura T, Miyajima A. 2003. Isolation of hepatoblasts based on the expression of Dlk/Pref-1. *J Cell Sci* **116:** 1775–1786.

Terauchi A, Johnson-Venkatesh EM, Toth AB, Javed D, Sutton MA, Umemori H. 2010. Distinct FGFs promote differentiation of excitatory and inhibitory synapses. *Nature* **465:** 783–787.

Tichelaar JW, Lu W, Whitsett JA. 2000. Conditional expression of fibroblast growth factor-7 in the developing and mature lung. *J Biol Chem* **275:** 11858–11864.

Tirnitz-Parker JE, Viebahn CS, Jakubowski A, Klopcic BR, Olynyk JK, Yeoh GC, Knight B. 2010. Tumor necrosis factor-like weak inducer of apoptosis is a mitogen for liver progenitor cells. *Hepatology* **52:** 291–302.

Turanyi E, Dezso K, Csomor J, Schaff Z, Paku S, Nagy P. 2010. Immunohistochemical classification of ductular reactions in human liver. *Histopathology* **57:** 607–614.

Turner N, Grose R. 2010. Fibroblast growth factor signalling: From development to cancer. *Nat Rev Cancer* **10:** 116–129.

Yamamoto-Fukuda T, Aoki D, Hishikawa Y, Kobayashi T, Takahashi H, Koji T. 2003. Possible involvement of keratinocyte growth factor and its receptor in enhanced epithelial-cell proliferation and acquired recurrence of middle-ear cholesteatoma. *Lab Invest* **83:** 123–136.

Yanger K, Stanger BZ. 2011. Facultative stem cells in liver and pancreas: Fact and fancy. *Dev Dyn* **240:** 521–529.

Yovchev MI, Zhang J, Neufeld DS, Grozdanov PN, Dabeva MD. 2009. Thymus cell antigen-1-expressing cells in the oval cell compartment. *Hepatology* **50:** 601–611.

Zhang L, Rubins NE, Ahima RS, Greenbaum LE, Kaestner KH. 2005. Foxa2 integrates the transcriptional response of the hepatocyte to fasting. *Cell Metab* **2:** 141–148.

Zong Y, Panikkar A, Xu J, Antoniou A, Raynaud P, Lemaigre F, Stanger BZ. 2009. Notch signaling controls liver development by regulating biliary differentiation. *Development* **136:** 1727–1739.

Neurochem Res (2012) 37:1898–1905
DOI 10.1007/s11064-012-0806-1

ORIGINAL PAPER

# Negative Regulation of Human Astrocytes by Interferon (IFN) α in Relation to Growth Inhibition and Impaired Glucose Utilization

**Ting Wang · Yasuhiro Takikawa · Kei Sawara · Yuichi Yoshida · Kazuyuki Suzuki**

Received: 16 February 2012 / Revised: 13 April 2012 / Accepted: 9 May 2012 / Published online: 25 May 2012


**Abstract** The present study assessed the direct effects of IFNs on human astrocytes. Human astrocytes were exposed to human recombinant IFNs, and the proliferation of cells was measured. Type I IFN receptor mRNA and protein expression, the phosphoprotein levels of signaling molecules including JNK, ERK1/2, IκB, p38MAPK, Stat3, and the expression of cytokines were determined respectively. In addition, cellular glucose consumption was measured as well as Glut-1 protein and activation of GSK-3β/mTOR signal were determined. The expression of Type I IFN receptor was detected in cultured human astrocytes. 2 IU/ml IFNα2a and IFNα2b significantly decreased the proliferation of human astrocytes respectively, compared to control. IFNβ had no significant effect on the proliferation of the cells. The phosphorylation of JNK stimulated by all IFNs detected was more pronounced and sustained than ERK1/2 and IκB. No effects were observed on the activation of p38MAPK and Stat3. Moreover, Treatment with IFNα, especially with IFNα2b, decreased glucose consumption and stimulated phosphorylation of GSK-3β and mTOR, but decreased the expression of Glut-1. In contrast, IFNβ had no significant effect on either glucose consumption or activation of GSK-3β/mTOR signals. INFα2b significantly decreased the levels of IL-8 whereas the levels of GM-CSF were increased. The present study demonstrates direct inhibitory effects of IFNα on cell proliferation, cell signaling and glucose utilization in human astrocytes.

T. Wang · Y. Takikawa · K. Sawara · Y. Yoshida · K. Suzuki (✉)
Division of Gastroenterology and Hepatology, Department of Internal Medicine, Iwate Medical University, Morioka, Iwate, Japan
e-mail: kasuzuki@iwate-med.ac.jp

**Keywords** IFNα-induced psychiatric side effects · Astrocyte proliferation · Glucose utilization · Cytokines · JNK · Glut-1

## Introduction

IFNα therapy is widely accepted for treating patients with hepatitis C virus (HCV). However, the tolerability of this treatment has been limited by high prevalence of side effects, especially psychiatric symptoms [1, 2]. A report by Trask et al. [1] suggests that opioid–dopamine changes, serotonin depletion, norepinephrine increase and endocrine dysfunction are responsible for those indirect actions of IFN. However, direct effects of IFN on the brain have not been given serious consideration, because IFN is not thought to readily cross the blood–brain-barrier (BBB) of the central nervous system (CNS) [3–5]. On the other hand, IFNα was shown to cause neuronal dysfunction in a laboratory study [6] and clinical reports reveal that IFNs are significantly increased in the CNS of human immunodeficiency virus (HIV) patients with dementia [7]. Therefore, a fuller understanding of the effects of IFN on CNS and BBB function at the cellular level is important to start to understand the basis of the neurological and psychiatric side-effects of IFNα.

Astrocytes play important roles in CNS function and in maintaining the BBB through their "end feet," which interact with structural components of the barrier. Recent studies have found that astrocytes determine both the functional as well as the structural architecture of the adult brain [8]. Furthermore, astrocytes are involved in the control of cognitive function in humans, having established roles in learning, perception, conscious integration, memory formation/retrieval and in the control of voluntary

behavior [9]. Abnormalities in the structure and dysfunction of astrocytes may lead to disruption of the BBB [10, 11], and astrocytic failure is implicated in the pathogenesis of a range of neurological disorders [12].

In addition, astrocytes play a central role in the control of brain energy metabolism [13] as supported by observations that glucose is taken up primarily by astrocytes in the brain in vivo [14], and that astrocytes take up half of the glucose from capillaries [15]. Astrocytes are distinguished from neurons in the CNS by taking up glucose from the circulation through the glucose transporter, Glut-1 [16].

Positron emission tomography (PET) using [F-18]-fluorodeoxyglucose (FDG) revealed that IFNα treatment impairs glucose uptake in patients with chronic hepatitis C virus infection [17].

In the current study, the cellular sensitivity of astrocytes derived a human-derived astrocyte cell line, to IFNs was identified by detecting the expression of type 1 interferon receptors. The effects of IFNs on cell proliferation and glucose utilization were then determined. The levels of cytokines in IFN-treated cultures were also determined since astrocytes have been shown to produce IFNs, tumor necrosis factor (TNF) α and other cytokines in response to viral infection and inflammation [18].

## Materials and Methods

### Cell Culture and Treatment

The human astrocyte cell line Cryo NHA (CLCC-2565) was purchased from Lonza Walkersville, Inc. in the USA. The cells were grown in a medium prepared using AGM BulletKit (CC-3186) as recommended by the manufacturer. The human hepatoblastoma cell line HepG2 was grown in DMEM supplemented with 10 % fetal bovine serum (FBS, Invitrogen), and were used as positive controls for the detection of IFN receptor expression. IFNα2a, IFNα2b, and IFNβ (Miltenyi Biotec) were added to the media at different concentrations, and the cells were incubated for different times as indicated.

### RT-PCR Analysis

Total RNA was extracted using RNAqueous-4PCR isolation kit (Ambion). Reverse transcription was performed by using high capacity cDNA reverse transcription kit (Applied Biosystems). Platinum PCR Supermix high fidelity (Invitrogen) was used. The following oligonucleotides were synthesized (FASMAC) and used as primers: IFNAR1 (sense 5′-TTTCAAGTTCAGTGGCTCCACGC-3′; antisense 5′-TCACAGGCGTGTTTCCAGACTG-3′); IFNAR2 (sense 5′-GAAGGTGGTTAAGAACTGTGC-3′; antisense 5′-CCCGCTGAATCCTTCTAGGACGG-3′). PCR was carried out for 30 cycles (denaturing at 94 °C for 30 s and annealing at 58 °C for IFNAR1, and at 54 °C for IFNAR2, respectively, for 30 s, and extension at 72 °C for 1.5 min [19]. The PCR products were separated by electrophoresis on a 1 % agarose gel and visualized after ethidium bromide staining under UV light.

### Evaluation of Viable Cells

Astrocytes were treated with or without 2 IU/ml IFNα subtypes and IFNβ, and incubated for 72 h. The number of viable astrocytes was evaluated using SF reagent (Nacalai Tesque Inc.) as previously reported [20]. Ten microliters of the cell count reagent SF were added to each well containing cultured astrocytes in 100 μl medium. The cells were incubated 1 h and the absorbance at 450 nm of the well was measured by a microplate photometer (Immuno-Mini NJ-2300 Inter Med). The changes in the cell number were arbitrary represented by a ratio of OD (optical density) of the stimulated cells divided by that of control cells.

### Bio-Plex Cytokine Assay

The supernatant fraction from IFN-treated cells was collected and analyzed by Bio-Plex cytokine assays (Bio-Plex Human Cytokine 18-Plex Panel, Bio-Rad Laboratories, Hercules, CA, USA), according to the manufacturer's protocol. The serum was analyzed for interleukin (IL)-1β, IL-2, IL-4, IL-5, IL-6, IL-7, IL-8, IL-10, IL-12, IL-13, IL-17, tumor necrosis factor (TNF) α, granulocyte-colony stimulating factor (G-CSF), granulocyte–macrophage colony-stimulating factor (GM-CSF), interferon (IFN)γ, macrophage inflammatory protein (MIP)-1b, and monocyte chemoattractant protein 1 (MCP-1).

### Bio-Plex Phosphoprotein Assay

The phosphorylation levels of the cell signaling proteins (p-JNK, p-p38MAPK, p-IκB-α, p-ERK2, and p-Stat3) in a single well of a 96-well microplate were measured using the Bio-Plex suspension array system (Bio-Plex human phosphoprotein 6-Plex Panel, Bio-Rad Laboratories). Briefly, the treated and untreated control cells were lysed according to the instructions specified in the Bio-Plex cell lysis kit product insert, and then the samples were analyzed according to the instructions specified in the Bio-Plex phosphoprotein assay instruction manual.

### Glucose Assays

The glucose concentrations in the incubation media were assessed by a quantitative enzymatic colorimetric kit (Bioassay systems), according the manufacturer's instructions.

Briefly, 5 μl aliquots of media were incubated with 100 μl of diagnostic glucose Trinder reagent, for 10 min at 37 °C and the absorbance read at 570 nm. A standard curve was prepared in the range of 0–1 mg/ml of D-glucose. Levels in each sample were calculated by interpolation from standard curves. Glucose utilization was determined as loss of glucose from the incubation media.

### Western Blot Analysis

Total protein was isolated from astrocytes by a total protein extraction kit purchased from BioChain Institute, Inc. Protein from each sample (10 μg) was separated by 10 % SDS-PAGE and electrotransferred onto a polyvinylidene difluoride membrane. Immunoblotting was performed by using specific antibodies against Glut-1(Abcam), anti-IFNAR1 antibody (Santa Cruz), p-IκB, β-actin (Santa Cruz Biotechnology), p-p38MAPK, p-ERK1/2, p-JNK, p-GSK-3β, p-mTOR, p-Stat3 (Cell signaling Technology). The immunoreactive bands were visualized with an enhanced chemiluminescence reagent (Amersham Biosciences).

### Statistical Analysis

Based on the results of Levene's test ($p > 0.05$), and a significant F-value, statistical analysis was carried out using the one-way ANOVA-POST HOC (Tukey's HSD) analysis in the SPSS statistics 17.0 software package (SPSS Japan Inc.). A $p$ value <0.05 was considered to be significant. Data are presented as the mean ± SD; median (25–75th percentile) unless otherwise indicated.

## Results

### Expression of IFN Receptors in Astrocytes

The type I IFN receptor contains at least two subunits; the IFNAR1 and the IFNAR2 [21, 22]. It was previously reported that HepG2 cells express the IFNAR subunits [23]. In the present study, the RNA expression of the IFNAR subunits was also detected in normal human astrocytes (Fig. 1a). In addition, the protein level of IFNAR1was detected using a specific antibody (Fig. 1b).

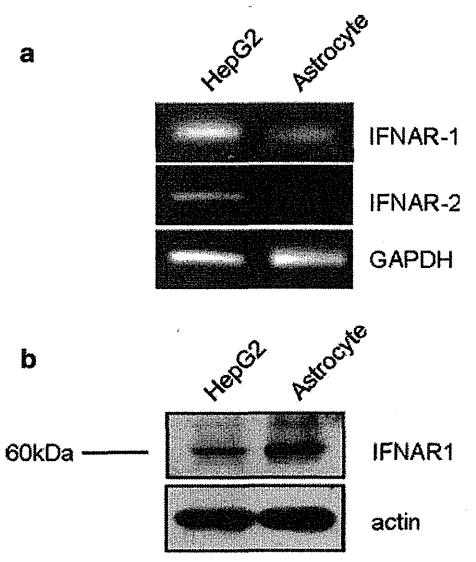


**Fig. 1** Expression of type I IFN receptors in astrocytes. **a** Expression of IFNAR1 and IFNAR2. Astrocytes and HepG2 cells were cultured to reach 80 % confluence. The total RNA was then isolated and RT-PCR was performed as described in "Materials and Methods". GAPDH served as an endogenous control. **b** The protein level of IFNAR1 was detected in astrocytes. The total cell lysate was prepared and a Western blot analysis was performed as described in "Materials and Methods". The level of β-actin was used as a loading control

### IFNα Inhibits the Proliferation of Astrocytes at a Concentration as Low as 2 IU/ml

The effect of 2 IU/ml of IFNα on the proliferation of astrocytes was investigated. IFNα2a and IFNα2b significantly decreased the proliferation of human astrocytes by 23 % ($p = 0.007$) and 13 % ($p = 0.02$), respectively, in comparison to the control (Fig. 2a). In contrast, 2 IU/ml IFNβ showed no significant effect on the proliferation of the cells. The phosphorylation of Mitogen Activated Protein Kinase (MAPK) family members (JNK, ERK1/2 and p38MAPK), and IκB, an inhibitory subunit of NF-κB, and Stat-3, are involved in the IFN-induced cell proliferation and apoptosis [24–26]. Long term treatment (72 h) of astrocytes with each IFN stimulated the activation of JNK. In addition, a relatively weak signal of p-ERK1/2 and p-IκB was also detected by both of IFNα subtypes (Fig. 2b). In contrast, there was no obvious activation of p38MAPK or Stat3 observed in the same study (data not shown). The effects IFNα2b in both dose–effect and short time course experiments were further tested by using a Western blot analysis and Bio-Plex phosphoprotein assay, respectively. The cells treated with different doses of IFNα2b for 72 h showed a stronger intensity of p-JNK rather than p-ERK1/2 or p-IκB (Fig. 2c). The short term stimuli by IFNα2b led to the activation of ERK1/2, JNK and IκB. However, IFNα2b affected neither p-p38MAPK nor p-Stat3 (Fig. 2d).

### IFNα2b Significantly Reduces Glucose Utilization by Astrocytes

There was no significant difference observed in the amount of glucose utilization between the cultures with and without the indicated IFN treatment after 2 h. However, the

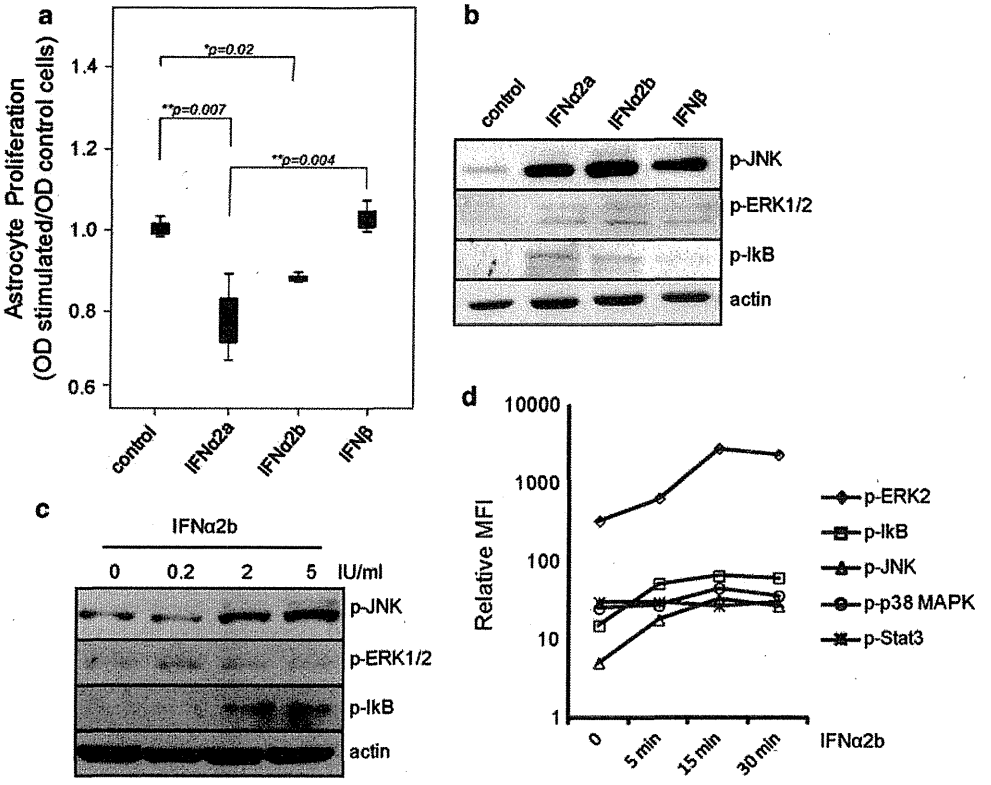


**Fig. 2** IFNα subtypes significantly inhibited the proliferation of astrocytes. **a** The effects of IFNs on the proliferation of astrocytes. $5 \times 10^4$/ml astrocytes were passaged into a 96-well plate in the culture medium. The cells were cultured 4 h and IFNs (2 IU/ml) and the vector as control were added into the cells respectively. The cells were incubated for 72 h thereafter, and the proliferation of astrocytes was evaluated using SF reagent. The data were presented as the median (25–75th percentile). n = 3, $*p < 0.05$; $**p < 0.01$ versus control. **b** The effects of IFNs on the stimulation of JNK, ERK1/2, IκB, p38MAPK and Stat3. The cells cultured in 6-well plate were starved for 4 h and then treated as described above. Cell lysates were prepared and collected for the Western blot analysis. The phosphorylation of indicated molecules was detected. The level of β-actin was used as a loading control. The experiments were repeated for 3 times and the representative data are shown. **c** The effects of IFNα2b on the activation of JNK, ERK and IκB in a dose–course study. IFNα2b with indicated concentration and a control vector were added to the starved astrocytes, respectively. The cells were cultured 72 h, collected and the signals were then detected by a Western blot analysis as described above. d. The effects of IFNα2b on the activation of JNK, ERK, IκB, p38MAPK and Stat3 in a time–course study. Astrocytes were cultured in 96-well plate and starved for 4 h before the treatment with 2 IU/ml IFNα2b. The cells were collected at each indicated time point and the intensity of phosphorylated ERK, IκB, JNK, p38MAPK, and Stat3 were measured by using Bio-Plex phosphoprotein assay as described in "Materials and Methods". The level of each phosphoprotein is indicated by the relative median fluorescence intensity (MFI), according to the manufacturer's instructions. The data are presented as the mean ± SD. n = 3

levels of glucose lost from the media decreased significantly after 4 h (16.9 %, $p < 0.05$) and 6 h (19 %, $p < 0.05$) in the cultures treated with IFNα2b in comparison to the controls. IFNα2a tended to decrease the glucose utilization by 7.8 % after 4 h and 12.5 % after 6 h. IFNβ slightly decreased the glucose utilization by 5 % after 6 h of treatment (Fig. 3a).

The protein expression levels of Glut-1was evaluated in the astrocytes with or without IFN stimulation. Glut-1 expression was detected in control cells. Both IFNα2b and IFNα2b markedly decreased the protein levels of Glut-1. Moreover, evaluating the phosphorylation of GSK-3β and mTOR, which are reported to participate in the negative regulation of the expression of Glut-1 [27], revealed that both IFNα2a and IFNα2b stimulated the activation of both factors. In contrast, IFNβ did not affect either the protein expression of Glut-1 or the phosphorylation of GSK-3β and mTOR (Fig. 3b). In addition, IFNα2b activated p-GSK-3β and p-mTOR inhibited the expression of Glut-1 in both a dose-dependent and time-dependent manner (Fig. 3c, d).

## Effects of IFNα Suptypes and IFNβ on the Levels of Cytokines in Astrocytes

The effect of IFN treatment on the levels of cytokines in the cells was evaluated. IL-6, IL-8, GM-CSF, MCP-1 and TNFα were detected in normal astrocytes (Fig. 4). Other cytokines, including IL-1β, IL-4, IL-10, G-CSF, MIP-1, IL-2, IL-5, IL-7, IL-10, IL-12, IL-13, IL-17 and IFNγ, showed low or undetectable levels in astrocytes. IFN

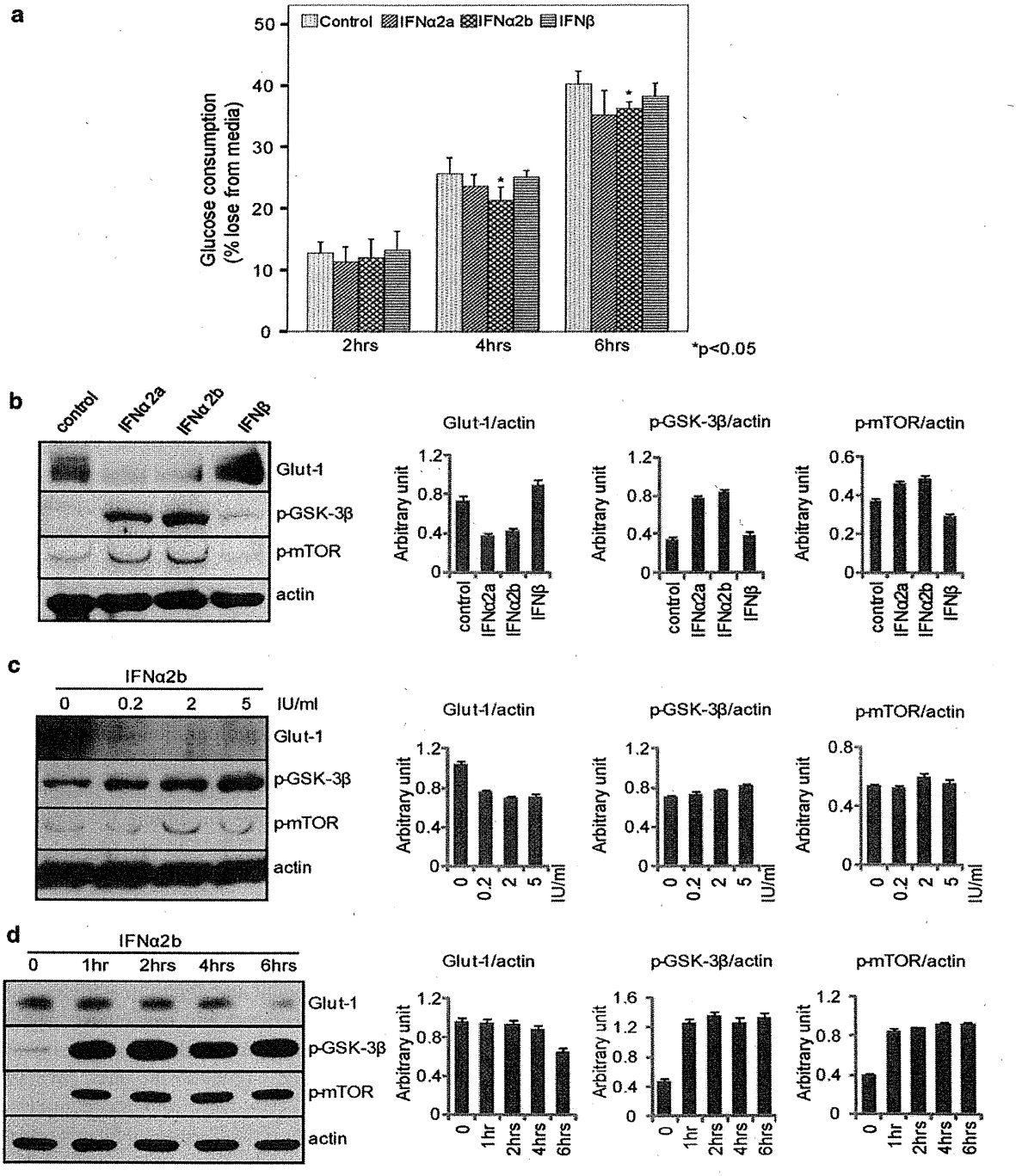


**Fig. 3** IFNα2b significantly inhibited the glucose utilization by astrocytes. **a** The effects of IFNs on the glucose utilization by astrocytes. Glucose consumption, assessed as loss of glucose from the incubation media, was measured after different times up to 6 h in the presence of 2 IU/ml IFNs or vector as control. Glucose levels in the culture media were measured at the indicated times. The data are presented as the mean ± SD of n = 3 replicates, and are expressed as % of glucose consumed. *$p < 0$ 0.05 versus control. **b** The effects of IFNs on the protein expression of Glut-1 and the activation of GSK-3$\beta$ and mTOR. Astrocytes were treated with various IFNs in a dose of 2 IU/ml for 72 h. **c**, **d**, The dose and time–course studies of IFNα2b. The cells were treated with IFNα2b as described in **a** and Fig. 2b. The expression level of Glut-1 and the phosphorylated GSK-3$\beta$ and mTOR were detected by a Western blot analysis. The level of $\beta$-actin was used as a loading control. The densitometric quantification of Western blots was performed using the ImageJ software program (NIH, USA). Experiments were performed three times, and the representative data was shown

treatment did not significantly change the levels of the detectable cytokines such as IL-6, MCP-1 and TNFα. However, IL-8 was significantly decreased by 38, 30, 40 % in the cultures treated with IFNα2a, IFNα2b and IFN$\beta$, respectively (n = 3, $p < 0.05$). In addition, the level of GM-CSF was significantly increased (1.2-fold compared to

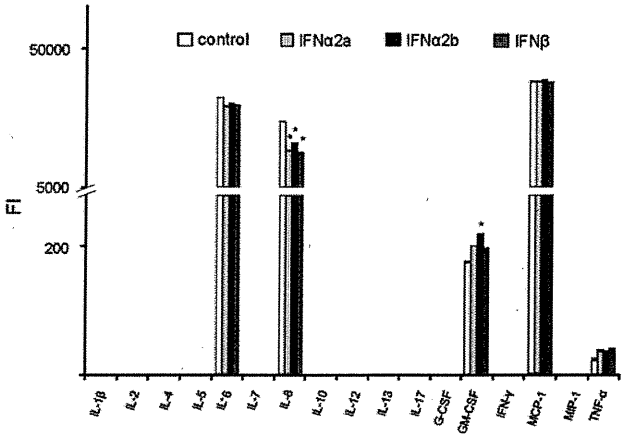


**Fig. 4** Effects of IFNs on the levels of cytokines produced in cultured astrocytes. Astrocytes were cultured and treated with indicated IFNs and control vector, respectively, under the same conditions described in Fig. 2b. The cell-free supernatant was collected and the cytokines were measured by using a Bio-Plex cytokine assay as described in "Materials and Methods". The level of each cytokine is indicated by the fluorescence intensity (FI), according to the manufacturer's instructions. The data were presented as the mean ± SD. n = 3. $^*p < 0.05$ versus control

the control, n = 3, $p < 0.05$) in the cultures treated with IFNα2b only.

## Discussion

Although the mitogenic activity of type II IFN (IFNγ) in astrocytes has been consistently reported [28, 29], the effect of type I IFN on the proliferation of this type of cell is unclear. Satoh et al. [30] reported that 50 or 100 IU/ml IFNα inhibits the proliferation of astrocyte-enriched cultures induced by IFNγ. The concentration of the IFNα subtypes used in our study is not more than 5 IU/ml (~25 pg/ml), which is within the range of the serum IFNα values for chronic hepatitis C patients who maintained a long-term response during IFN treatment [31]. Therefore, the effects of IFNα observed in the present study are considered to be much closer to the actual clinical conditions.

Recently, the FDA approved pegylated interferon-alpha, in which polyethylene glycol is added to make the interferon last longer in the body. (Pegylated interferon-alpha-2b was approved in January 2001; pegylated interferon-alpha-2a was approved in October 2002.) The current study showed that both IFNα2a and IFNα2b inhibit the proliferation of astrocytes, and that IFNα2a showed stronger inhibitory effects than IFNα2b, thus indicating the possibility that IFNα may have toxic effects on the function and/or survival of astrocytes.

IFNα2a and IFNα2b share the ability to bind to type 1 IFN receptors, which are involved in signal transduction [22, 32, 33]. The IFNAR1 subunit is associated with Tyrosine Kinase (TYK)-2, and IFNAR2 is associated with JAK1 [34]. In addition, P38MAPK is also regulated by IFN signaling via JAK activation [35]. However, the molecular mechanism underlying the effects of IFN on astrocytes is still unclear. In our study, although IFNAR expression was detected in astrocytes, the levels of the phosphorylated p38MAPK and Stat3, one of the downstream factors of JAK that regulates spinal astrocytes proliferation [36] did not change significantly by IFN treatment. Instead, both temporary and long term stimulation with IFNα2b markedly induced the activation of JNK. This data indicates that IFN activates signal transduction in astrocytes via a JAK/Stat3 independent pathway. Despite the JAK pathway, other signaling pathways activated by type I IFNs have been elucidated. For example, IFNα induces JNK activation, in combination with ERK activation, resulting in apoptosis in human KB cells [37]. In contrast, IFN induces NF-κB activation to mediate cell survival in Daudi B lymphoma cells, which are widely employed as a model of IFNα-induced growth inhibition [38]. The activation of JNK was markedly stimulated by long term treatment with IFNα in the current study, in comparison to ERK1/2 or NF-κB. Data suggest that the prolonged activation of JNK may play a role in the IFN- induced inhibition of astrocyte proliferation.

On the other hand, IFNβ (0–100 ng/ml) exerts a dual role in regulating the proliferation of astrocytes, and NFκB activation is necessary for the IFNβ reaction [39]. High doses of IFN-beta (50 or 500 IU/ml) inhibit the proliferation of human astrocytes in culture [30]. The current data showed that 2 IU/ml IFNβ did not significantly affect the proliferation of astrocytes. Besides, there was no obvious activation of IκB. Therefore, the action of IFNβ may be dose dependent.

Energy-dependent processes are the basis for metabolic imaging of functional and cognitive activities of the brain. IFN treatment decreases glucose uptake in patients with hepatitis C, and the present data supportively showed that both IFNα subtypes inhibited the short-time (0–6 h) glucose utilization of astrocytes from the cultured medium to a larger degree than IFNβ. Glut-1 silencing results in the inhibition of cell proliferation and glucose uptake [40]. The protein expression of Glut-1 decreased not only in response to the long term (72 h) treatment with IFNα subtypes in the current study, but also decreased shortly after 4 h treatment with IFNα2b. These data therefore, suggest that Glut-1 suppression may relate to the negative effects of IFN on glucose utilization by astrocytes. Studies in renal tubular and laryngeal tumor cells revealed that Glut-1 is negatively regulated by GSK-3/TSC2/mTOR signaling [27]. The current data show that IFNα stimulated both GSK-3β and mTOR while decreasing Glut-1 expression, indicating that the two molecules may participate in the IFNα-mediated suppression of Glut-1 in astrocytes.

Cytokines are known for their ability to regulate cell survival in addition to immune responses. Recent reports reveal that the pro-inflammatory cytokines IL-1, IL-6, and TNFα can serve as mitogens for bovine astrocytes in culture [28, 29]. On the other hand, pro-inflammatory cytokines (IL-1β, IL-6, IFNγ and TNFα) increase glucose utilization in astrocytes, while anti-inflammatory cytokines like IL-4 and IL-10 decrease astrocytic glucose utilization [41]. The present data shows that IFN treatment did not affect the expression levels of the cytokines addressed above, indicating that the effects of IFNα on astrocytes does not require intermediary cytokines. However, the data show that IFNα2b treatment significantly suppresses the levels of IL-8 but elevates the levels of GM-CSF, both belonging to the family of chemokines. There are limited reports on the function of the chemokines in the CNS. Astrocytes express IL-8 under normal circumstances [42], indicating that a normal concentration of IL-8 is essential for the survival and normal function of these cells. On the other hand, active astrocytes produce GM-CSF in response to inflammatory signals and therefore may induce a cycle of immune dysregulation and BBB breakdown [43]. The involvement of the regulation of these two cytokines in the function of IFNα needs to be further clarified.

The novelty of our study, in brief, is to demonstrate that IFNα exerts an inhibitory effect on human astrocytes with a concentration that mimics the clinical conditions. Especially, this is the first report to describe the inhibitory effects of IFNα on glucose utilization by astrocytes. Given the key role played by the astrocyte as a component of the neurovascular unit and BBB, alterations in cellular function, cellular signaling and energy metabolism resulting from exposure of these cells to IFNα with concentrations that mimic clinical conditions, if replicated in vivo, could result in impaired astrocytic function. Consequent alterations in astrocyte–neuron coupling leading to altered neural excitability could underlie some of the neuropsychiatric complications of IFN therapy in Hepatitis C patients.

**Acknowledgments** We thank Professor Roger F. Butterworth for his kind editing and great advice on our manuscript. We thank Ms. A. Watanabe for her valuable technical assistance. This study was supported by the Japan Society for the Promotion of Science, and a Grant-in-Aid for Scientific Research (No. 21590857).

**Conflict of interest** The authors declare that they have no conflict of interest.

## References

1. Trask PC, Esper P, Riba M, Redman B (2000) Psychiatric side effects of interferon therapy: prevalence, proposed mechanisms, and future directions. J Clin Oncol 18:2316–2326
2. Malek-Ahmadi P, Hilsabeck RC (2007) Neuropsychiatric complications of interferons: classification, neurochemical bases, and management. Ann Clin Psychiatry 19:113–123
3. Habif DV, Lipton R, Cantell K (1975) Interferon crosses blood-cerebrospinal fluid barrier in monkeys. Proc Soc Exp Biol Med 149:287–289
4. Smith RA, Norris F, Palmer D, Bernhardt L, Wills RJ (1985) Distribution of alpha interferon in serum and cerebrospinal fluid after systemic administration. Clin Pharmacol Ther 37:85–88
5. Billiau A (1981) Interferon therapy: pharmacokinetic and pharmacological aspects. Arch Virol 67:121–133
6. Sas AR, Bimonte-Nelson H, Smothers CT, Woodward J, Tyor WR (2009) Interferon-alpha causes neuronal dysfunction in encephalitis. J Neurosci 29:3944–3955
7. Rho MB, Wesselingh S, Glass JD, McArthur JC, Choi S, Griffin J, Tyor WR (1995) A potential role for interferon-alpha in the pathogenesis of HIV-associated dementia. Brain Behav Immun 9:366–377
8. Nedergaard M, Ransom B, Goldman SA (2003) New roles for astrocytes: redefining the functional architecture of the brain. Trends Neurosci 26:523–530
9. Pereira A Jr, Furlan FA (2010) Astrocytes and human cognition: modeling information integration and modulation of neuronal activity. Prog Neurobiol 92:405–420
10. Sofroniew MV (2000) Astrocyte failure as a cause of CNS dysfunction. Mol Psychiatry 5:230–232
11. Eugenin EA, Clements JE, Zink MC, Berman JW (2011) Human immunodeficiency virus infection of human astrocytes disrupts blood-brain barrier integrity by a gap junction-dependent mechanism. J Neurosci 31:9456–9465
12. Seifert G, Schilling K, Steinhauser C (2006) Astrocyte dysfunction in neurological disorders: a molecular perspective. Nat Rev Neurosci 7:194–206
13. Voutsinos-Porche B, Bonvento G, Tanaka K, Steiner P, Welker E, Chatton JY, Magistretti PJ, Pellerin L (2003) Glial glutamate transporters mediate a functional metabolic crosstalk between neurons and astrocytes in the mouse developing cortex. Neuron 37:275–286
14. Chuquet J, Quilichini P, Nimchinsky EA, Buzsaki G (2010) Predominant enhancement of glucose uptake in astrocytes versus neurons during activation of the somatosensory cortex. J Neurosci 30:15298–15303
15. Nehlig A, Coles JA (2007) Cellular pathways of energy metabolism in the brain: is glucose used by neurons or astrocytes? Glia 55:1238–1250
16. Turner DA, Adamson DC (2010) Neuronal-astrocyte metabolic interactions: understanding the transition into abnormal astrocytoma metabolism. J Neuropathol Exp Neurol 70:167–176
17. Takikawa Y, Wang T, Sawara K, Suzuki K (2011) Interferon-α inhibits the proliferation of human astrocyte and decreases the expression of glucose transporter Glut-1. J Gastroenterol Hepatol 26:144 (Abstract)
18. Lee SC, Liu W, Dickson DW, Brosnan CF, Berman JW (1993) Cytokine production by human fetal microglia and astrocytes. Differential induction by lipopolysaccharide and IL-1 beta. J Immunol 150:2659–2667
19. Matsumoto K, Okano J, Murawaki Y (2005) Differential effects of interferon alpha-2b and beta on the signaling pathways in human liver cancer cells. J Gastroenterol 40:722–732
20. Ishiyama M, Miyazono Y, Sasamoto K, Ohkura Y, Ueno K (1997) A highly water-soluble disulfonated tetrazolium salt as a chromogenic indicator for NADH as well as cell viability. Talanta 44:1299–1305
21. Novick D, Cohen B, Rubinstein M (1994) The human interferon alpha/beta receptor: characterization and molecular cloning. Cell 77:391–400